Zoological Journal of the Linnean Society, 2024, **201**, zlae097
https://doi.org/10.1093/zoolinnean/zlae097
Advance access publication 10 August 2024
Original Article

OXFORD

Original Article

Cranial anatomy of the Triassic rhynchosaur *Mesosuchus browni* based on computed tomography, with a discussion of the vomeronasal system and its deep history in Reptilia

William Foster[1,*], Paul Gensbigler[1], Jacob D. Wilson[1], Roger M. H. Smith[2,3], Tyler R. Lyson[3,4] and Gabriel S. Bever[1,3,4,5,*]

[1]Center for Functional Anatomy and Evolution, Johns Hopkins University School of Medicine, 1830 East Monument Street, Baltimore, MD 21215, USA
[2]Karoo Palaeontology, Iziko South African Museum, PO Box 61, Cape Town 8000, South Africa
[3]Evolutionary Studies Institute, University of the Witwatersrand, 1 Jan Smuts Avenue, Braamfontein 2000, Johannesburg, South Africa
[4]Department of Earth Sciences, Denver Museum of Nature & Science, 2001 Colorado Boulevard, Denver, CO 80205, USA
[5]Department of Earth and Planetary Sciences, 3400 North Charles Street, Johns Hopkins University, Baltimore, MD 21218, USA

[*]Corresponding author. Center for Funtional Anatomy and Evolution, Johns Hopkins University School of Medicine, 1830 East Monument Street, Baltimore, Maryland, MD 21215, USA. E-mail: wfoster7@jh.edu

[*]Corresponding author. Center for Funtional Anatomy and Evolution, Johns Hopkins University School of Medicine, 1830 East Monument Street, Baltimore, Maryland, MD 21215, USA. E-mail: gbever1@jhmi.edu

ABSTRACT

The stem lineage of Archosauria is populated by a diverse fossil record that remains notably understudied relative to the crown clade. Prominent among these specimens is a beautifully preserved skull of the early mid-Triassic rhynchosaur *Mesosuchus browni* [Iziko South African Museum (SAM) 6536], whose phylogenetic position has considerable influence on patterns of pan-archosaurian cranial evolution. We used high-resolution, micro-computed tomography to re-examine the anatomy of this specimen, building on previous studies that were either limited to external observations or restricted to the braincase. A digital segmentation of the cranial elements and primary neurovascular canals of SAM-PK-6536 allows for expanded character scoring and constitutes a foundation for future comparative insights. Our data support the phylogenetically oldest instance of a pneumatized maxilla in a pan-archosaur, bringing the record of antorbital pneumatization into closer alignment with that of the neurocranium. The nasal cavity and primary palate of *Mesosuchus* includes a complex septomaxilla, a novel element anterior to the vomer, and is likely to have supported a well-developed vomeronasal system. The evolution of this system is discussed in terms of both phylogenetic pattern and how the skeletal architecture of *Mesosuchus* and other fossils could inform the signalling dynamics that pattern the vomeronasal system during development.

Keywords: Archosauria; computed tomography; cranial anatomy; Rhynchosauria; sensory evolution; Triassic; vomerolfaction

INTRODUCTION

The Permo-Triassic sediments of the Karoo Basin in South Africa have yielded a host of important pan-archosaur fossils, supporting a descriptive literature that stretches back more than a century (e.g. Broom 1903, 1913a). Among these discoveries are the earliest rhynchosaurs, an extinct clade of herbivorous reptiles that appear as small-bodied forms in the Early Triassic (Ezcurra *et al.* 2016), undergo diversification in the Middle Triassic (Ezcurra *et al.* 2020), and are extinct by the end-Triassic (Norian: Benton 1990, Allen *et al.* 2019). Phylogenetic analyses place Rhynchosauria as an early divergence from the stem of Archosauria (i.e. a non-archosauriform pan-archosaur lineage), with *Mesosuchus browni* Watson, 1912 (hereafter simply *Mesosuchus*) representing one of the basal-most splits within the group (Mukherjee and Ray 2014, Butler *et al.* 2015, Schultz *et al.* 2016, Ezcurra *et al.* 2020, Sues *et al.* 2020). This topology conveys considerable influence to *Mesosuchus* for inferring character evolution both within Rhynchosauria and along the backbone lineage that produced the archosaur crown clade.

Received 29 March 2024; revised 26 June 2024; accepted 10 July 2024

Mesosuchus is known from four specimens (Dilkes 1998), all from the Early–Mid-Triassic *Cynognathus* Assemblage Zone of the Karoo Supergroup (Hancox *et al.* 2020). The holotype locality is positioned at the base of the *Trirachodon–Kannemeyeria* Subzone (Hancox *et al.* 2020) and currently regarded as early Anisian (Wolvaardt *et al.* 2023). The holotype specimen occurs in the same sandstone block as the type specimen of *Euparkeria capensis* Broom, 1913, with the two forms originally conflated as one taxon (Watson 1912). Morphological support for two taxa was compiled by Broom (1913), who noted a general similarity between *Mesosuchus* and the rhynchosaurs *Howesia browni* Broom, 1905, *Rhynchosaurus articeps* Owen, 1842, and *Hyperodapedon gordoni* Huxley, 1859, all of which were considered rhynchocephalian lepidosaurs at the time. Further preparation of the original block yielded a second specimen, and continued quarrying for dimension stone at the locality produced two more (Haughton 1922, Wolvaardt *et al.* 2023). One of the latter specimens, SAM-PK-6536 (Haughton 1924), includes a fully articulated and undistorted skull that Broom (1925) considered one of the finest fossils ever found (Fig. 1). SAM-PK-6536 also includes a series of articulated cervical vertebrae and ribs, dorsal vertebrae and ribs, left scapulocoracoid, right scapula, distal end of a left humerus, interclavicle, clavicles, and gastralia (Dilkes 1998).

Although SAM-PK-6536 is frequently included in comparative works (e.g. Romer 1956, Malan 1963, Kuhn 1969, Carroll 1976, 1988), the definitive description is that by Dilkes (1998). This thorough and careful study, which covers all four specimens of *Mesosuchus*, is hampered only by the absence of X-ray computed tomography (CT) and the access these data provide to internal anatomy. The work of supplementing Dilkes (1998) with CT-driven insights began with the braincase (Sobral and Müller 2019, see also Wilson *et al.* 2022).

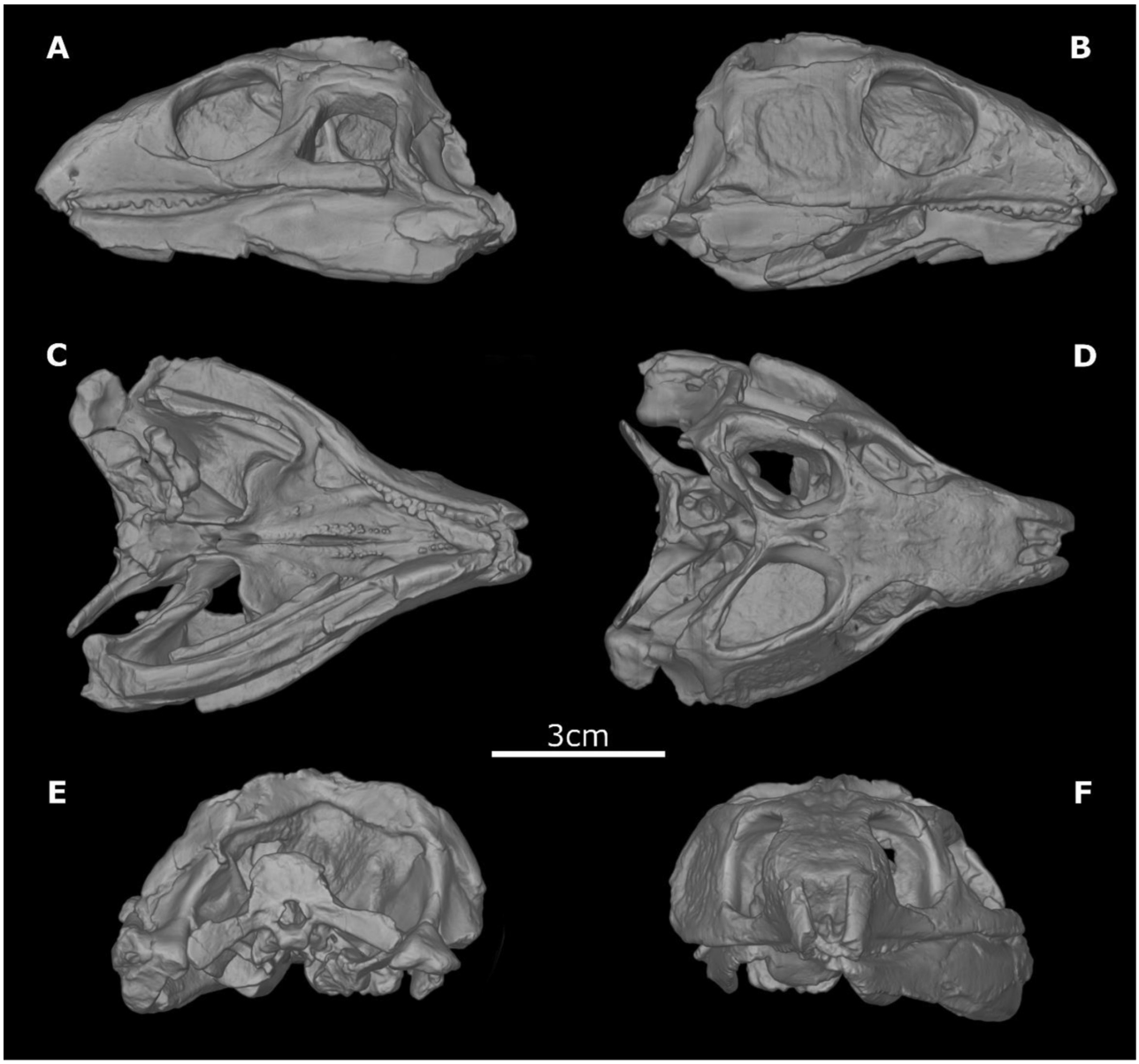

Figure 1. Volume renderings of the skull of SAM-PK-6536, *Mesosuchus browni*, in: A, left lateral; B, right lateral; C, ventral; D, dorsal; E, posterior; and F, anterior views.

Here, we continue these efforts by describing the remaining (non-braincase) regions of the skull, with a focus on those features not visible to Dilkes (1998). Of particular note is the presence of maxillary air cells that we interpret as pneumatic, and the anatomy of the nasal cavity and palate, which bear clear evidence of a well-developed vomeronasal system (VNS). We assess the evolutionary implications of our data through broad-based comparisons that inform character transformations along both the phylogenetic backbone of the archosaur total group (hereafter referred to as Pan-Archosauria) and within Rhynchosauria. The size and identity of the comparative sample is largely shaped by the availability of CT-based studies for stem archosaurs, which is growing but is still a poor reflection of known taxonomic and morphological diversity.

MATERIALS AND METHODS

Computed tomography scanning and segmentation

SAM-PK-6536 was scanned in 2010 at the University of Texas High-resolution X-ray CT facility. A total of 1122 coronal sections were acquired at 1024 × 1024 resolution and maximum field of view 74.7766 mm. Image processing included re-slicing along sagittal and horizontal planes, three-dimensional reconstruction, and digital segmentation of all non-braincase elements, all using Amira (v.6.3.0). Both right and left sides of paired elements were segmented. All slice data and additional animations are available at: https://n2t.net/ark:/87602/m4/616700

Comparisons and phylogenetic analysis

Generalized polarization of observed variation was established by direct comparison with a number of taxa that bracket *Mesosuchus* phylogenetically (Fig. 2). These taxa include the diapsid stem reptile *Youngina capensis* Broom, 1914 (Gow, 1974), the putative stem testudine *Eunotosaurus africanus* Seely, 1892 (Bever *et al.* 2015), the early stem archosaur *Macrocnemus bassanii* Nopcsa, 1930 (Miedema *et al.* 2020), crownward stem archosaurs *Prolacerta broomi* Parrington, 1935 (Modesto and Sues 2004) and *Euparkeria capensis* (Sookias *et al.* 2020), and a series of other rhynchosaurs. Comparisons in the text will be based on the initial citation for the respective taxon unless otherwise noted. Open-source CT data of taxa used for comparisons are detailed in the Supporting Information (Table S1).

We reanalysed the phylogenetic matrix of Scheyer *et al* (2020; which, in turn, is derived from Ezcurra 2016) with adjusted scorings for *Mesosuchus*. We conducted a 'new technology search' using Wagner trees in TNT (v.1.6), as recommended by Goloboff and Morales (2023) for large matrices. Tree bisection and reconnection (TBR) branch swapping, sectorial searches, Ratchet, and Tree Fusing were all activated. Following Scheyer *et al.* (2020), we searched until 100 hits of the same minimum tree length were found. The resultant trees were saved to RAM and subjected to a second round of TBR branch swapping using the 'traditional search option' in TNT. Bremer support and bootstrap values were calculated using the built-in functions in TNT. We also reanalysed the rhynchosaur-focused phylogenetic matrix of Ezcurra (2016) (derived from Butler *et al.* 2015). We ran a 'traditional search' with 10 000 replications. Bremer support and bootstrap values were calculated using the built-in functions in TNT. A list of resultant cranial apomorphies diagnosing selected clades for both analyses is provided as Supporting Information (Appendix S1).

Anatomical abbreviations

Abbreviations used in the labelling of anatomical features in figures are as follows: **addf**, adductor fossa; **afp**, articular fossa for premaxilla; **agpm**, anterior groove on the maxilla for the

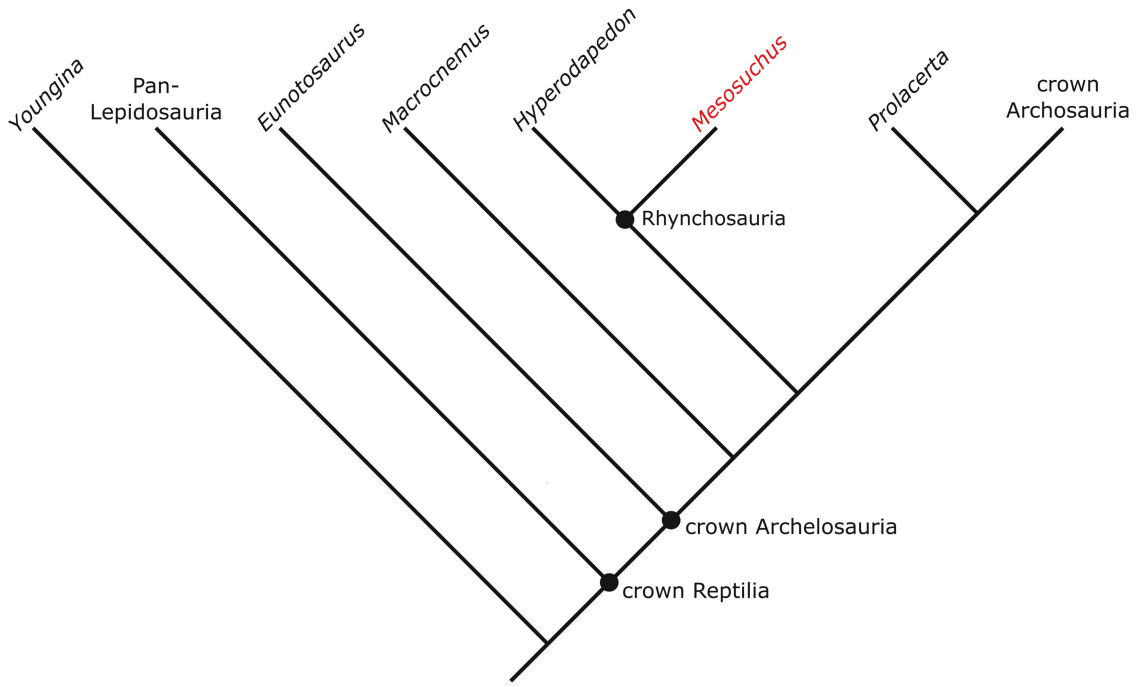

Figure 2. Schematic tree displaying the generally accepted phylogenetic relationships of the taxa we use for general comparisons in our description of *Mesosuchus browni*.

reception of the premaxilla; **amf**, anterior maxillary foramen; **amy**, anterior mylohyoid foramen; **ang**, angular; **aobi**, accessory olfactory bulb impression; **art**, articular; **asfl**, anterior surangular foramen lateral opening; **asfm**, anterior surangular foramen medial opening; **bc**, braincase; **cc**, caudal canal of maxilla; **ceri**, cerebellar impression; **choa**, choana; **cor**, coronoid; **cpmc**, caudal posteromedial canal of maxilla; **cpmf**, caudal posteromedial foramen of the maxilla; **dent**, dentary; **dnf**, neurovascular foramina of the dentary; **dt**, dentary teeth; **elp**, element P; **fmr**, jugal medial ridge; **fr**, frontal; **glf**, glenoid fossa; **iac**, inferior alveolar canal; **iacmc**, medial canal of inferior alveolar canal; **icm**, internal chambers of maxilla; **info**, infraorbital fenestra; **jc**, jugal canal; **Jch**, Jacobson's chamber; **jlf**, jugal lateral foramina; **jmf**, jugal medial foramen; **l. ect**; left ectopterygoid; **l. elp**, left element P; **l. ep**; left epipterygoid; **l. jug**, left jugal; **l. lac**, left lacrimal; **l. max**, left maxilla; **l. nas**, left nasal; **l. pal**, left palatine; **l. pm**, left premaxilla; **l. po**, left postorbital; **l. pof**; left postfrontal; **l. prf**; left prefrontal; **l. q**, left quadrate; **l. qj**; left quadratojugal; **l. sq**, left squamosal; **l. st**, left supratemporal; **l. vom**, left vomer; **lac**, lateral canals in maxilla; **lacd**, lateral canals of dentary; **laf**, lateral foramina of the maxilla; **ljc**, lateral canals of jugal; **lsmc**, lateral foramen in septomaxilla; **ltf**, lower temporal fenestra; **mjc**, medial canal of jugal; **mkf**, Meckelian fossa; **mkg**, Meckelian groove; **mt**, maxillary teeth; **nlc**, nasolacrimal canal; **oltg**, olfactory tract groove; **opbi**, optic lobe impressions; **orb**, orbit; **pa**, parietal; **palg**, palatine groove; **part**, prearticaular; **pdpd**, posterodorsal process of dentary; **pf**, parietal foramen; **piaf**, posterior inferior alveolar foramen; **pmfr**, premaxillary fragment; **pmy**, poster mylohyoid foramen; **pnpn**, paranasal plate of nasal; **pobi**, posterior olfactory bulb impression; **prff**, prefrontal foramen; **psfg**, posterior surangular foramen; **pt**, pterygoid; **pvpd**, posteroventral process of dentary; **qf**, quadrate foramen; **r. ect**, right ectopterygoid; **r. elp**, right element P; **r. ep**, right epipterygoid; **r. fr**, right frontal; **r. jug**, right jugal; **r. lac**, right lacrimal; **r. max**, right maxilla; **r. nas**, right nasal; **r. pm**, right premaxilla; **r. po**, right postorbital; **r. pof**; right postfrontal; **r. prf**; right prefrontal; **r. q**; right quadrate; **r. sq**, right squamosal; **r. st**, right supratemporal; **r. vom**, right vomer; **rpmc**, rostral posteromedial canal of maxilla; **rpmf**, rostral posteromedial foramen of the maxilla; **sac**, superior alveolar canal; **sang**, surangular; **smx**, septomaxilla; **sof**, suborbital fenestra; **spc**, splenial canal; **spl**, splenial; **sppc**, posterior canal of splenial; **stf**, supratemporal fenestra; **vt**, vomerine teeth.

RESULTS

Description

Dermal roofing elements

The nasal is a paired element that contacts the premaxilla and maxilla laterally, lacrimal posteromedially, prefrontal posterolaterally, frontal posteriorly, and the contralateral nasal along the sagittal midline (Figs 3–6). The posterior suture with the frontal is concave in dorsal view but assumes a more transverse orientation ventrally. This is potentially autapomorphic, because the dorsal expression of the same suture in all other rhynchosaurs is also transverse [e.g. *Rhynchosaurus articeps* (Benton 1990) and *Hyperodapedon gordoni* (Benton 1983)]. The structure of the nasals includes two basic components: (i) a horizontal, dorsal plate that roofs the nasal cavity anteriorly and forms the deeply concave posterior margin of the largely undivided external nares; and (ii) a vertical, paranasal plate that lines the dorsolateral wall of the nasal cavity (anterior to the prefrontal, lacrimal, and ascending process of the maxilla) (Fig. 5A). This paranasal plate is long, perhaps autapomorphically so, and almost completely excludes the premaxillae from the external nares, tapering to a point immediately behind the anterior extent of that element. The dorsal plate is pierced by several small canals that open into the nasal cavity (Fig. 6) and are likely to have transported superficial branches of the ophthalmic nerve (V1) (as in other crown reptiles: Oelrich 1956, Werner 1962, Lessner and Holliday 2022a, b). The strongly concave shape of the posterior margin of the external naris appears to be an autapomorphy of *Mesosuchus*.

The paired prefrontal is a triangular element (in lateral view), formed by anterior, posterodorsal, and ventrodorsal processes (Figs 3–6). The anterior process forms an abutting, dorsomedial contact with the nasal, a rostral point contact with the premaxillae, and is overlapped slightly by the ascending processes of the maxillae ventrally. The contact with the nasal is dorsoventrally shallow and contrasts with the deep, reinforced suture observed in rhynchosaurids (e.g. *Rhynchosaurus articeps* and *Hyperpodapedon gordoni*). The posterodorsal process extends along the anterolateral margin of the frontal, and the posteroventral process overlaps the lacrimal and narrows to a point contact with the jugal. Exclusion of the lacrimal from the orbit by the prefrontal is a plesiomorphic condition shared with *Rhynchosaurus articeps*, whereas the lacrimal forms the entire anterior margin of the orbit in more deeply nested rhynchosaurs [e.g. *Bentonyx sidensis* Langer *et al*, 2010 (Sethapanichsakul *et al.* 2023a) and Hyperodapedontinae]. The prefrontal is only exposed narrowly in dorsal view, as in *Rhynchosaurus articeps*. This condition is plesiomorphic relative to the derived condition in more deeply nested rhynchosaur taxa, wherein the element is mediolaterally expanded (e.g. *Bentonyx sidensis* and Hyperodapedontinae). In addition to dominating the anterior margin of the orbit, the prefrontal contributes to a large medial (i.e. internal) concavity, whose roof and floor are completed by the frontal and lacrimal, respectively (Figs 5A, 6). This space is inferred to have housed olfactory components of the telencephalon (see Discussion). A single foramen is present on the lateral surface of the anterior process and proceeds as a blind canal anteroposteriorly within the posterodorsal process (Fig. 5B).

The frontal is a paired, plate-like, roughly quadrangular bone that contacts the nasal anteriorly, prefrontal anterolaterally, postfrontal posterolaterally, and parietal posteriorly (Figs 3–6). The frontal–parietal contact is deeply interdigitating and transverse, without the prominent convexity found in many stem archosaurs (e.g. *Prolacerta broomi*). The outer surface exhibits a longitudinal excavation that extends the entire length of the bone (Fig. 5B). In *Rhynchosaurus articeps* and *Bentonyx sidensis* these excavations are restricted to the posterior quadrant of the bone, whereas in Hyperodapedontinae they exhibit a transverse orientation at the mid-length of the bone. The ventral surface exhibits an elongate, descending process that defines an hourglass-shaped median space that was occupied by the cerebrum (posteriorly) and olfactory structures anteriorly (Fig. 6) (see Discussion). This space

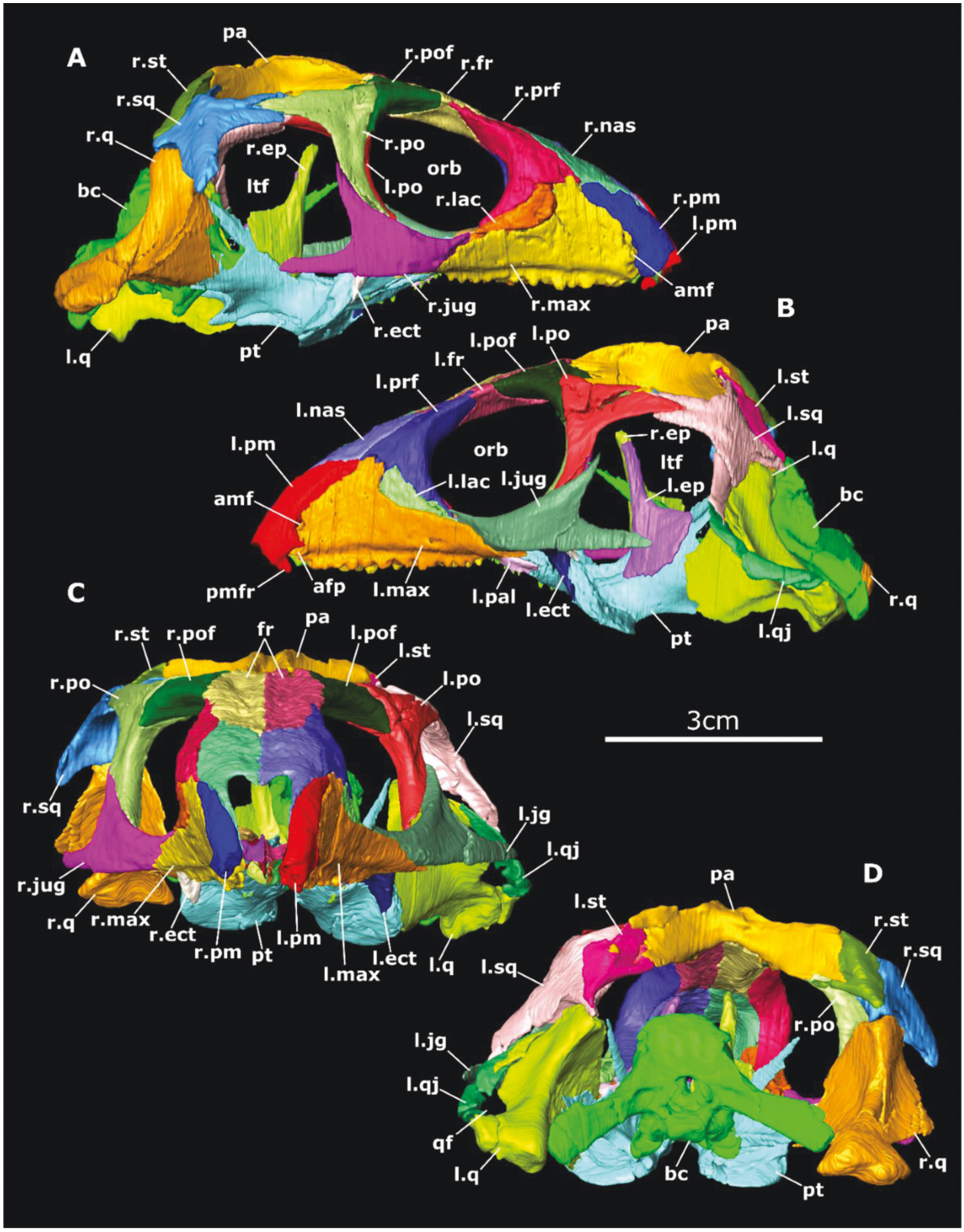

Figure 3. Digitally segmented skull of SAM-PK-6536, *Mesosuchus browni*, in: A, right lateral; B, left lateral; C, anterior; and D, posterior views.

is confluent anteriorly with that already described for the prefrontal.

The parietals are fused into a single midline element contacting the frontals, postfrontals, and postorbitals anteriorly and the squamosals and supratemporals posterolaterally. Structural details are well described by Dilkes (1998); we add only the presence of distinctive impressions on the posteroventral surface of the element (labelled 'opbi' in Fig. 6). The entire region

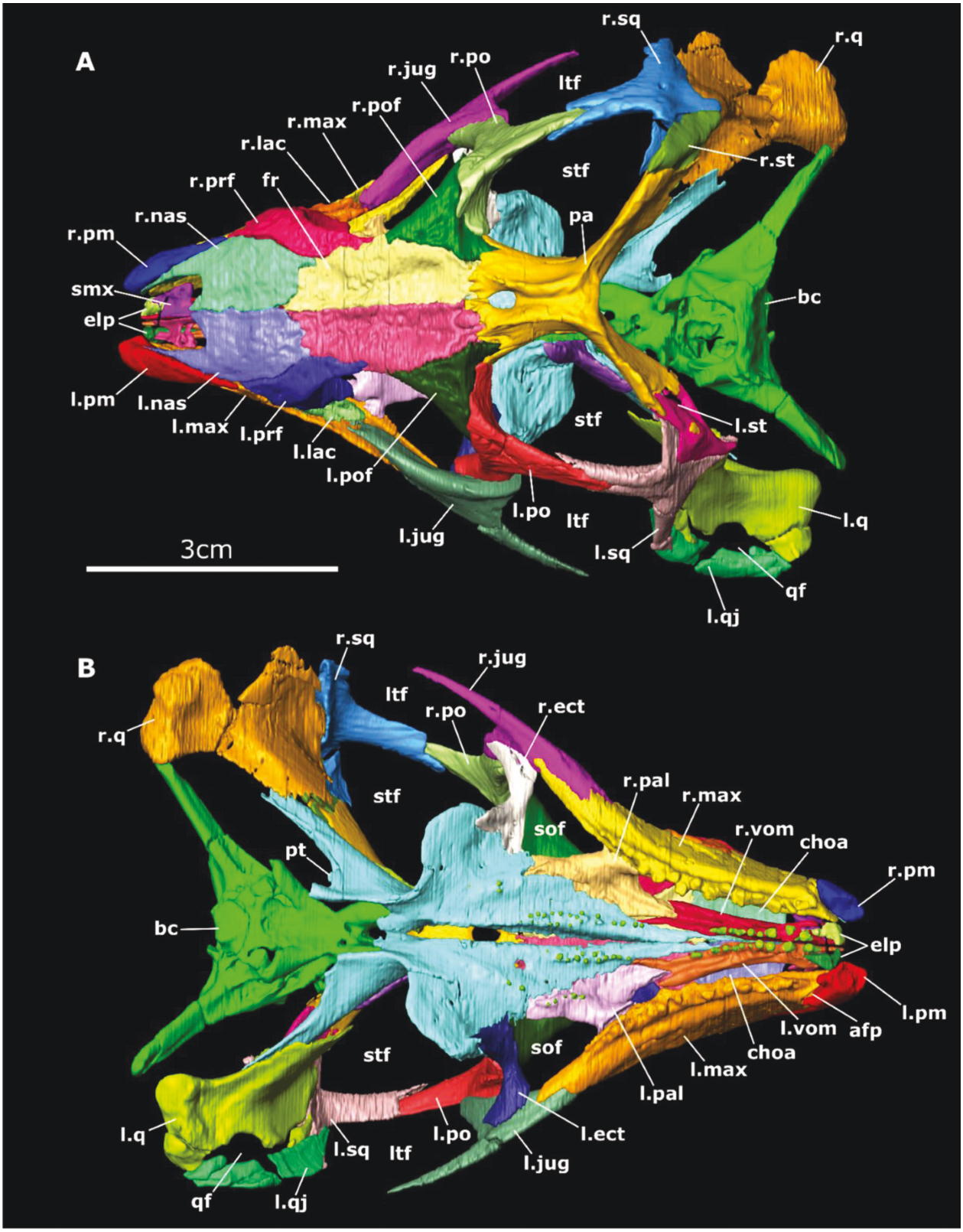

Figure 4. Digitally segmented skull of SAM-PK-6536, *Mesosuchus browni*, in: A, dorsal; and B, ventral views.

posterior to the parietal foramen is deeply concave. This region of the parietal is occupied by the optic lobes in extant lepidosaurs (Allemand *et al.* 2023) and crocodylians (Lessner *et al.* 2022a). This wider concavity is posteriorly confluent with a mediolaterally restricted pit that lies at the sagittal midline of the parietal. A similar structure is identified in the rhynchosaurid *Hyperodapedon gordoni*, although this impression is located further anteriorly, at about the level of the parietal foramen, and

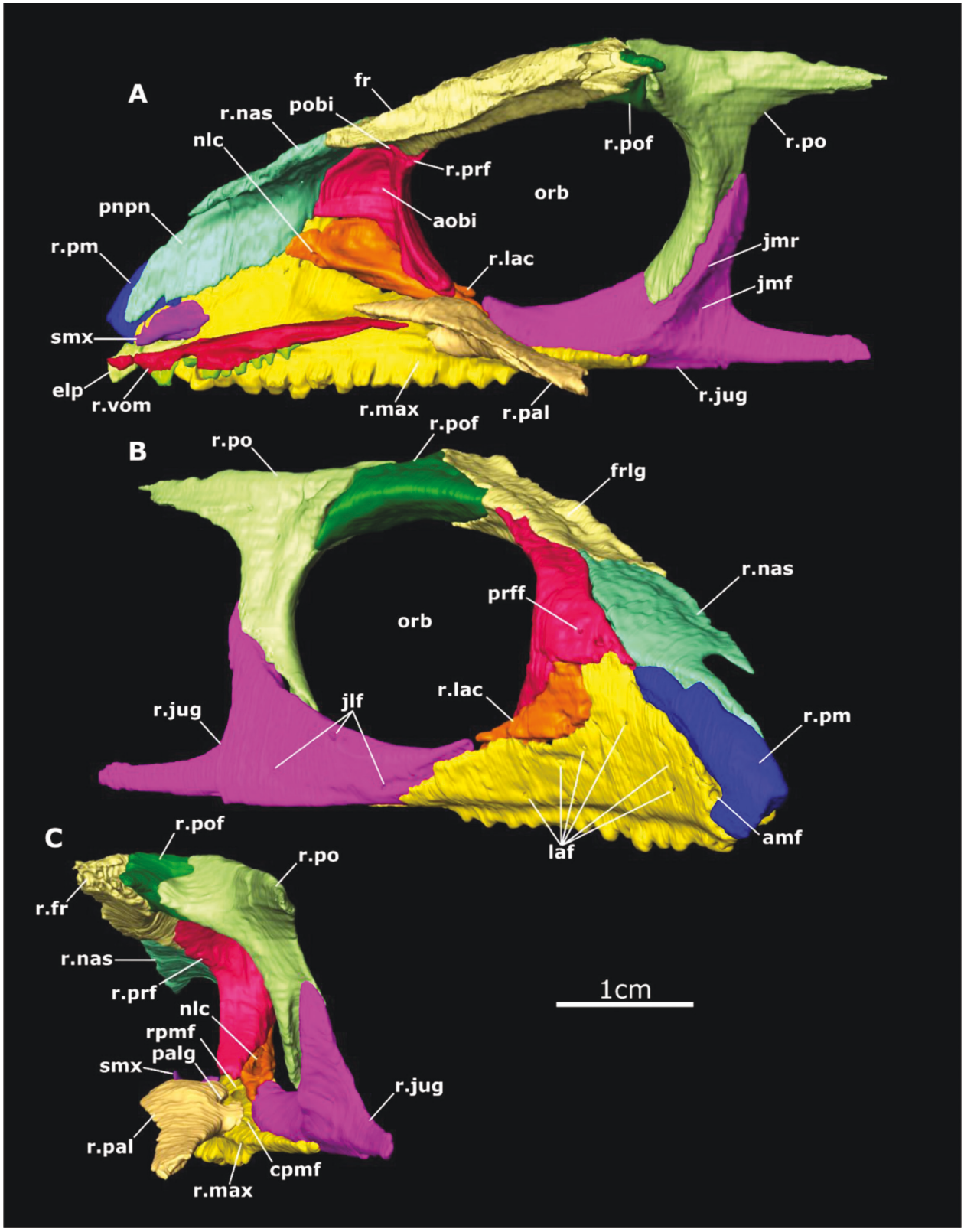

Figure 5. Digitally isolated rostrum and orbital bones of SAM-PK-6536, *Mesosuchus browni*, in: A, medial; B, anterolateral; and C, posterior views.

might well be an impression of the pineal organ (Benton 1983: fig. 4). A small pit at around the mid-length of the parietal was identified in the rhynchosaurid *Teyumbaita sulcognathus* Azevedo and Schultz, 1987(Sales and Schultz 2014: fig. 2). Given the spatial relationship of this pit to the optic lobes in *Mesosuchus*, it might be an impression of the cerebellum itself.

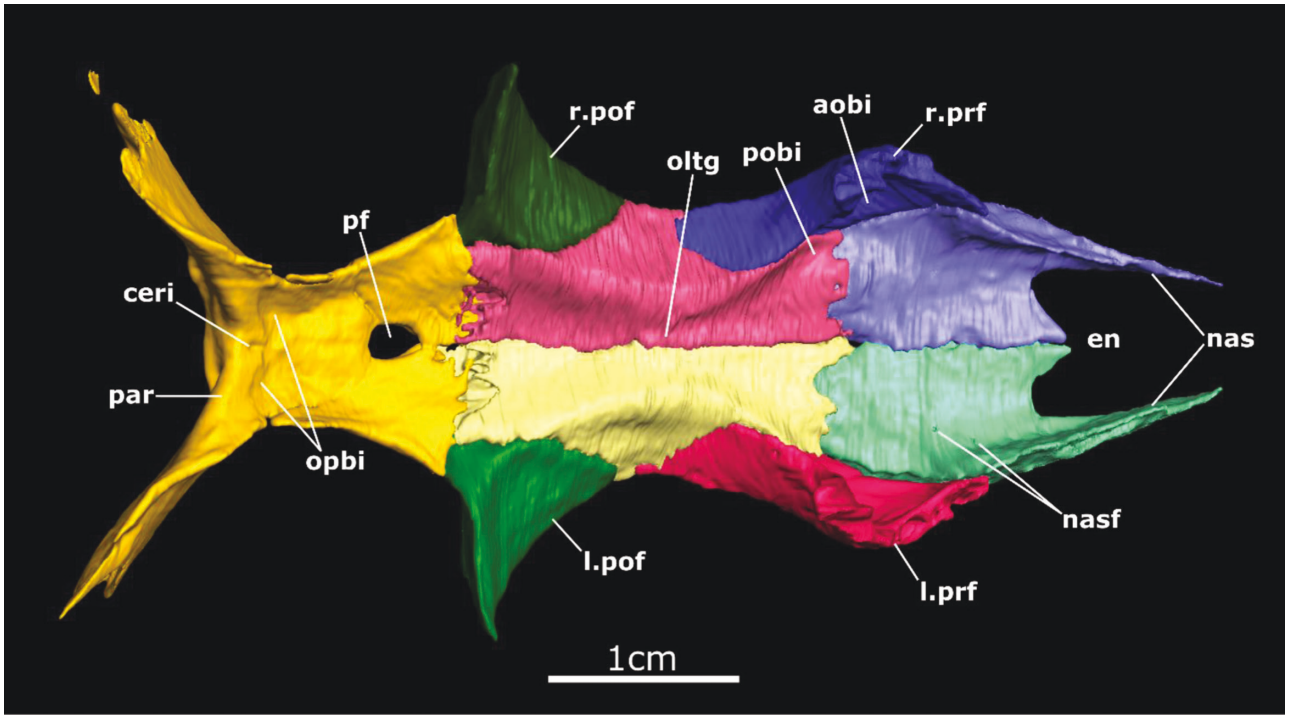

Figure 6. Digitally isolated skull roof bones of SAM-PK-6536 in ventral view.

Its small size would be comparable to the cerebellum of extant lepidosaurs and crocodylians.

The paired jugal is triangular, with gracile anterior, posterior, and posterodorsal processes (Figs 3–5). The anterior process extends along the medial surface of the maxilla, resting on the medial maxillary shelf. The horizontal alignment of jugal and maxilla is a plesiomorphic feature of *Mesosuchus* shared, for example, with *Eohyosaurus wolvaardti* Butler *et al*, 2015 (Butler *et al.* 2015). This is unlike the condition in *Rhynchosaurus articeps*, *Langeronyx brodiei* Benton, 1990 (Chatterjee 1974), *Stenaulorhynchus stockleyi* Haughton, 1932 (von Huene 1938), and *Hyperodapedon gordoni*, wherein the jugal is robust overall, wedge shaped, and mediolaterally expanded such that it is visible in dorsal view. The anterior process of *Rhynchosaurus articeps* retains the gracile morphology found in *Mesosuchus*. The distal length of the jugal contacts both the lacrimal and prefrontal. This process is broadly concave in lateral view, reflecting its ventral contribution to the orbit. The anterior process contacts the posterolateral surface of the lacrimal and shares a short medial contact with the lateral process of the palatine. The posterior process lacks bony contacts, extending approximately halfway along the ventral margin of the lower temporal fenestra to form an incomplete lower temporal bar. The posterodorsal process runs obliquely across the lateral surface of the postorbital, joining that element in forming the postorbital bar and thus the anterior margin of the lower temporal fenestra. This is unlike the condition in *Eohyosaurus wolvaardti* and Hyperodapedontinae, wherein the jugal forms the entire anterior fenestral margin. The lower temporal bar in *Mesosuchus* is incomplete, as in *Eohyosaurus wolvaardti*. This contrasts with the morphology in Rhynchosauridae, wherein the bar is completed by the posterior process of the jugal and the anterior process of the quadratojugal (e.g. *Rhynchosaurus articeps*, *Hyperodapedon gordoni*). In medial view, the body of the jugal (i.e. the confluence of these three processes) is traversed by a distinctive, oblique ridge that continues onto the posterodorsal process and clearly separates the anterior, orbital portion of the jugal from its posterior contribution to the adductor chamber (Fig. 5A). The medial surface of the body of the jugal shares an abutting contact with the concave lateral surface of the ectopterygoid (Fig. 4B). The lateral surface of the jugal is pierced by several small neurovascular foramina (Fig. 4A, B) that converge internally into a single canal, which then bifurcates to send branches into both the anterior and dorsal processes (Fig. 5B). A branch of this canal exits medially into the adductor chamber. Given its spatial association with the adductor chamber, this canal is likely to have transported fibres of the maxillary artery (see Canal sections). The jugal of SAM-PK-6536 lacks a prominent 'anguli-oris crest', a structure that is also lacking in non-rhynchosaurian stem archosaurs and that was first interpreted as the attachment surface of the m. levator anguli oris of squamates (Sill 1971). There is, however, no consensus regarding its identity (Benton 1983).

The paired lacrimal is positioned within the posterior rostrum, where it is sandwiched (in lateral view) between the prefrontal posterodorsally and the maxilla anteroventrally (Figs 3–5). Much of the lacrimal rests on the narrow, medial maxillary shelf. From this position, the lacrimal contacts the posteroventral margin of the nasal and lateral process of the palatine. A posterior contact with the jugal negates a maxillary contribution to the orbit, although the orbital contribution of the lacrimal is itself largely negated by the overlying prefrontals. As noted by Dilkes (1998), the nasolacrimal canal is restricted to the lacrimal, opening in the orbit through a pair of foramina and in the nasal cavity via a single foramen (Fig. 5A, C).

The paired postfrontal is a triangular, wedge-shaped element in lateral view (Figs 3, 4, 6), whose size is less than half that of the postorbital. A relatively small postfrontal is shared with other rhynchosaurs and is unlike the plesiomorphic condition wherein the postfrontal and postorbital are roughly equivalent in size [e.g. *Macrocnemus bassanii* and *Azendohsaurus madagaskarensis* Flynn *et al.*, 2010 (Flynn *et al.* 2010)]. Contacts include a simple but rostrocaudally elongate medial suture with the frontal, a shorter, interdigitating, medial suture with the parietal, and a broad, overlapping, lateral suture with the postorbital. The postfrontal forms the posterodorsal corner of the orbit and makes a smaller contribution to the supratemporal fossa. The dorsal surface is deeply pitted, with CT confirming these pits as superficial.

Computed tomography data reveal a largely complete left quadratojugal (Figs 3, 4). The simple, strap-like element that Dilkes (1998) identified as the right quadratojugal, we interpret as a dislocated fragment of the lateral quadrate. This conclusion is based on its identical thickness to the contralateral quadrate and the fragmented nature of its medial border. The posteroventral end of the left quadratojugal lies against the lateral surface of the quadrate (immediately dorsal to the articular condyle). Anterodorsally, the quadratojugal extends along the anterolateral margin of the quadrate to rest against the anterior edge of the squamosal at the ventral-most extent of that element. The paired squamosal contacts the postorbital anteriorly, quadrate and quadratojugal ventrally, and parietal and supratemporal posterolaterally (Figs 3–5). The supratemporal is a paired, plate-like, transversely oriented bone that is restricted to the occipital surface (Figs 3, 4). It lies against the posterior surface of the squamosal and parietal, where these bones join to form the post-temporal bar. Lateroventral contact with the quadrate is negated by a small process of the squamosal, as in *Rhynchosaurus articeps* but unlike *Hyperodapedon gordoni* and *Hyperodapedon sanjuanensis* Sill, 1970 (Gentil and Ezcurra 2022), wherein the supratemporal is absent.

Palatal elements

The paired premaxilla is narrowly overlapped by the maxilla along an elongate posterior suture, forms a point contact with the prefrontal posterodorsally, and bears a long, plate-like suture with the nasal medially (Figs 3–5). The contact with the maxilla is distinctly notched and is pierced by a sizeable foramen that opens into the superior alveolar canal (Figs 3, 4) (see Maxilla and Canal sections). A second, more ventral foramen noted by Dilkes (1998) is, in fact, an articular fossa in the maxilla for the posteroventral extent of the premaxilla and does not communicate with any internal spaces (Figs 3A, 4B). The dorsolateral overlapping of the premaxilla by the maxilla is unlike the condition in the stem archosaurs *Macrocnemus bassanii* and *Prolacerta broomi*, wherein the premaxilla overlaps the maxilla.

There is no preserved midline contact with the contralateral premaxilla, including along the alveolar margin (no preserved subnarial bar). *Mesosuschus* is reconstructed with the plesiomorphic sub-narial bar formed by medial processes of the premaxilla (e.g. *Macrocnemus bassanii*) (Dilkes 1998). The subnarial bar of rhynchosaurids is formed not by medial processes of the premaxilla but by the robust fusion of the medial surfaces of the premaxillary 'beak', which is entirely edentulous. This condition might, in part, reflect damage, but it seems unlikely that the robust midline suture of deeply nested rhynchosaurids (e.g. *Hyperodapedon gordoni*) was present, especially given that the bar is missing in other early rhynchosaurids [e.g. *Noteosuchus* Broom, 1925 (Carroll 1976), *Howesia browni* (Dilkes 1995), and *Eohyosaurus wolvaardti*]. The alveolar process is oriented horizontally and houses a single, large tooth alveolus. The fragment of a second, more posterior premaxillary tooth proposed by Dilkes (1998) appears to be a broken, slightly displaced fragment of the premaxilla itself (Fig. 3B). The premaxilla of the holotype (*SAM-PK-5882*) clearly houses a second tooth, potentially indicative of intraspecific variation.

The paired maxilla is a broadly triangular element with distinctive posterior and anterodorsal processes (Figs 3–5). Contacts include the premaxilla anteriorly, prefrontal dorsally, jugal posteriorly, lacrimal posteromedially, and nasal, vomer, and palatine medially (Figs 3–5). The curved anterior surface of the element includes a deep groove that accepts both the premaxilla and the prefrontal. The medial surface includes a narrow but elongate shelf that supports the overlying lacrimal and meets the palatine and vomer. This shelf appears to be lacking in *Youngina capensis* and *Eunotosaurus africanus*, and among pan-archosaur taxa stemward of rhynchosaurs. Its presence in *Prolacerta broomi* and *Euparkeria capensis* suggests a synapomorphy of rhynchosaurs and crownward pan-archosaurs. We interpret the dorsal extensions of the vomer described by Dilkes (1998: p. 508) as the septomaxilla for reasons listed below. The maxilla forms nearly the entire lateral margin of the choana but is excluded from the orbit by lacrimal–jugal contact. This choanal contribution is a plesiomorphic feature shared with *Rhynchosaurus articeps*, *Bentonyx sidensis*, and *Hyperodapedon hueni* (Langer and Schultz 2000) but is excluded by a derived vomer–palatine contact in *Hyperodapedon gordoni* and *Hyperodapedon sanjuanensis*. The sizeable foramen that pierces the premaxillary suture opens into the large and complex superior alveolar canal. The narrow feeding surface houses a row of 16 teeth, long considered of ankylothecodont implantation (Watson 1912, Broom 1913, Haughton 1922, Malan 1963) (see Discussion).

As mentioned earlier, the dorsal extensions of the vomers described by (Dilkes 1998) are here interpreted as well-preserved septomaxillae (Figs 3–9; see also Gentil and Ezcurra 2022). These paired, anterior elements include a saddle-like main body, a sizeable lateral process, and an even larger medial process. The lateral process abuts the maxilla, whereas the contralateral medial processes form a midline crest. The lateral and medial processes impart a broadly concave shape to the dorsal surface of the element, which opens into the greater nasal cavity. The ventral surface features the right and left halves of a broad midline concavity that separates the septomaxillae from the underlying vomers and a pair of more anterior ossifications of uncertain homology (elements P, see below). The septomaxilla forms no direct contacts with these ventral bones. The intervening space is confluent with a canal that exits the septomaxillae through their lateral processes (Figs 7, 8). The space is also confluent with the choanae and thus connects with the oral cavity (Fig. 7A).

A paired ossification of uncertain homology lies within the anterior palate (Figs 3, 4, 7–9). We refer to these symmetric

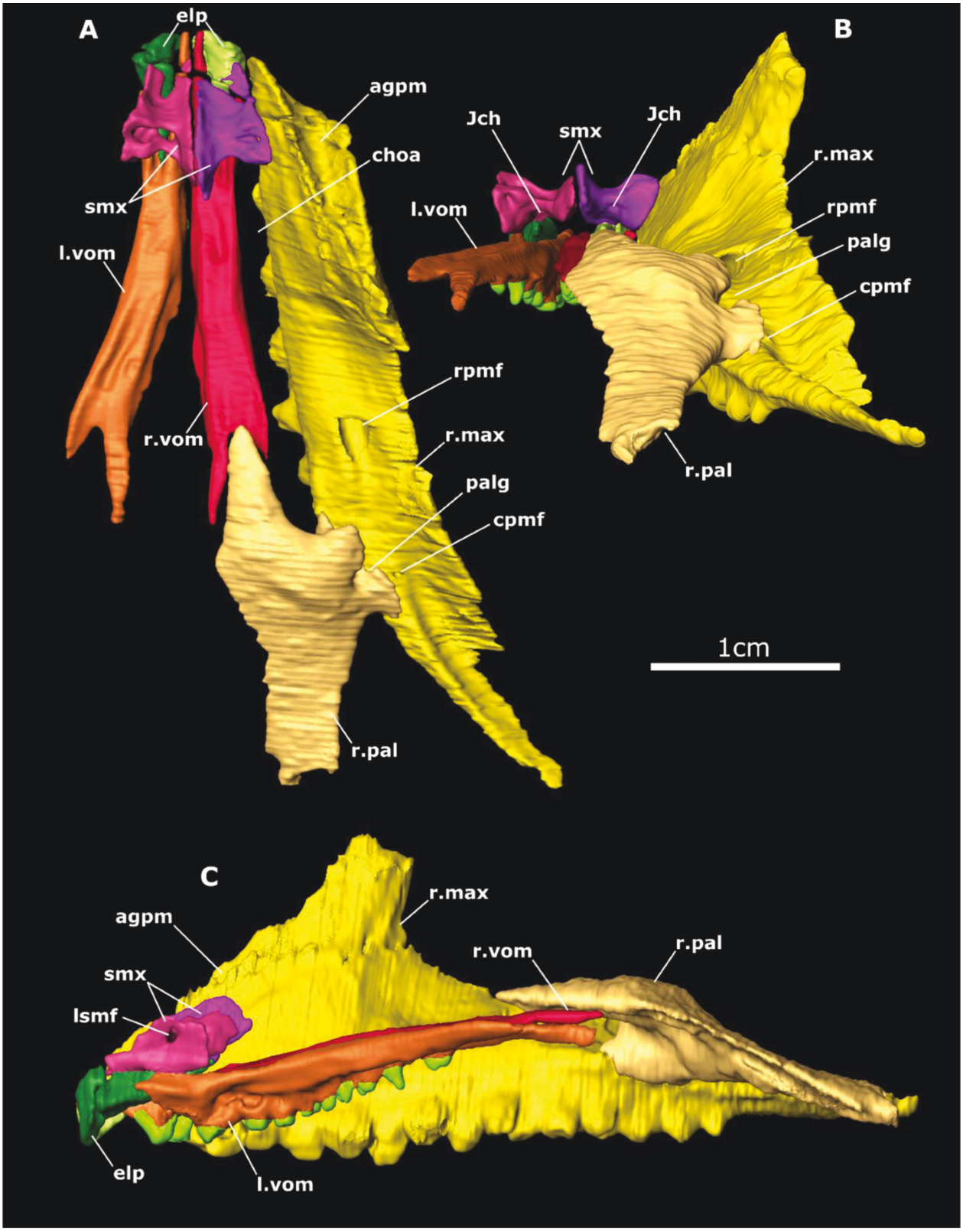

Figure 7. Digitally isolated palatal region of SAM-PK-6536, *Mesosuchus browni*, in: A, dorsal; B, posterior; and C, medial views.

bones simply as elements P ('P' because of their association with the palate) until a more satisfactory nomenclature is established (see Discussion). The elements are hook shaped in lateral view, reflecting a concave anteroventral margin. Posteriorly, each bone tapers to a sharp point and shares indirect contacts with the tines of the anterior vomerine fork. Each element P is surrounded by the premaxilla and maxilla laterally and the septomaxilla dorsally, although there is no direct contact with any of these

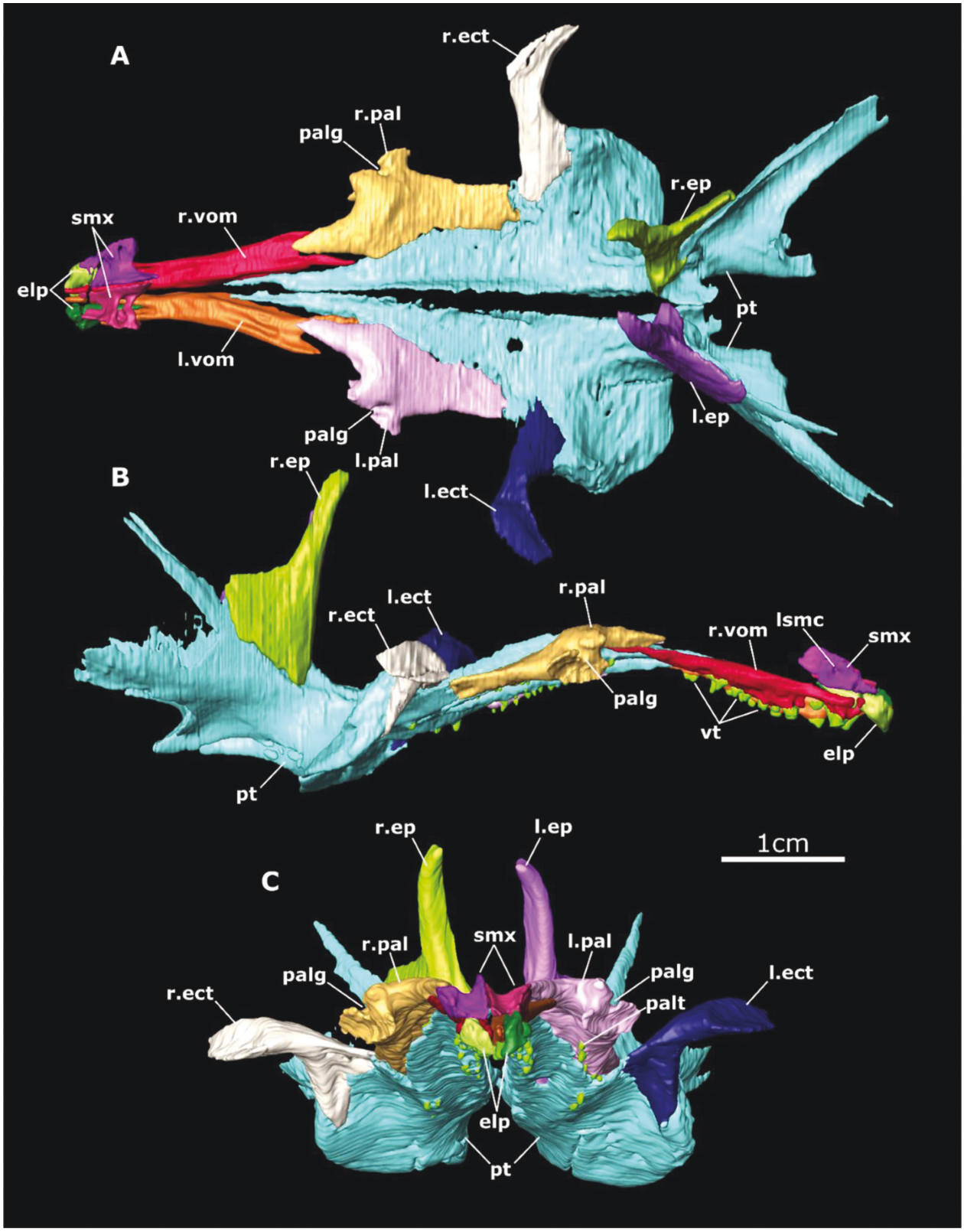

Figure 8. Digitally isolated palatal complex of SAM-PK-6536, *Mesosuchus browni*, in: A, dorsal; B, right lateral; and C, anterior views.

elements. The only direct contact is the deeply interdigitating suture with the vomer posteriorly.

The paired vomer is an elongate element that flares at its anterior and posterior ends, both of which are distinctly forked in their formation of deeply interdigitating sutures with the palatines and elements P, respectively (Figs 4, 7–9). Other bony contacts include the maxilla anterolaterally, pterygoid posteriorly, and a long, midline, contralateral suture that ends posteriorly

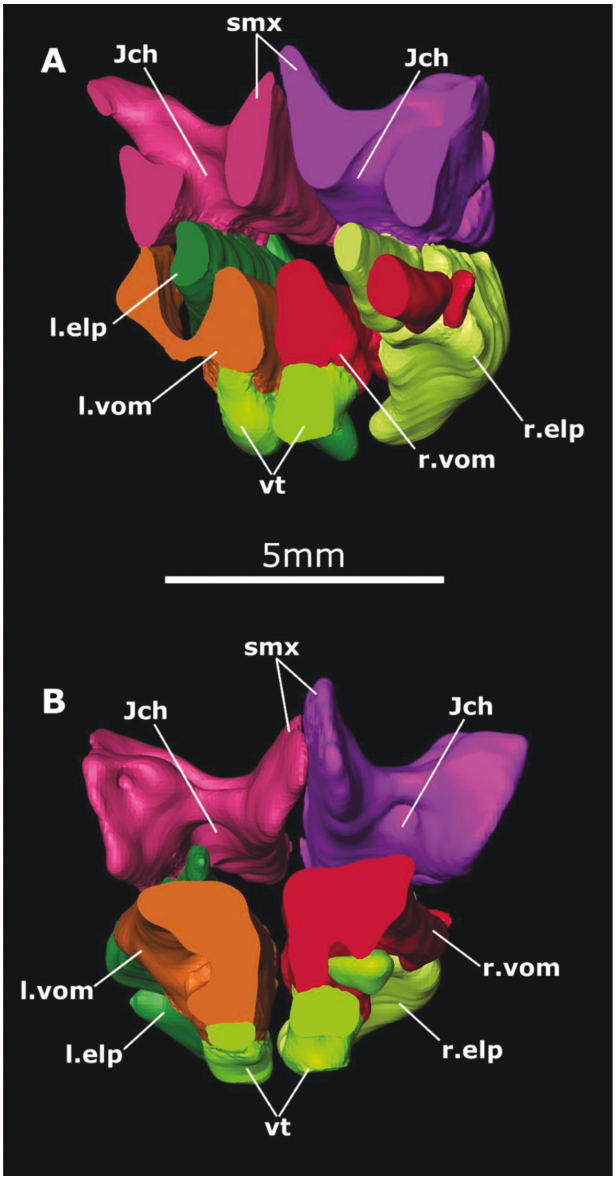

Figure 9. Digitally isolated septomaxilla of SAM-PK-6536, *Mesosuchus browni*, in coronal section: A, through centre of Jacobson's chamber in posterolateral view; and B, through vomer in posterior view.

where the two elements divide to accept collectively the rostral ends of the palatines. The anterior end of the vomers produces a midline, dorsal concavity that continues forward onto elements P. The short and rather weak contact with the anteromedial surface of the maxillae completes the anterior margin of the choana. Both vomers possess a single row of teeth along the sagittal midline.

The palatine is a paired element of the posterior palate that includes anterior and lateral processes (Figs 4, 7, 8). The flat, finger-like anterior process forms an interdigitating contact with the vomers anteriorly, whereas the more robust lateral process forms an abutting contact centred on the maxilla but extending posteriorly onto both the lacrimal and the jugal. Medially, there is an elongate, slightly overlapping suture with the pterygoid that largely mirrors the oblique orientation of the posterior palate as a whole. The transverse, posterior margin is narrowly separated from the ectopterygoid by the pterygoid. The palatine forms the posterior margin of the choana and nearly the entire medial margin of the suborbital fenestra. The suborbital fenestra is triangular (Fig. 4B), unlike the condition in rhynchosaurids, which possess small, circular openings (e.g. Benton 1990, Gentil and Ezcurra 2022). The condition in *Mesosuchus* is similar to that of the early stem testudine *Eunotosaurus africanus*. Palatine teeth are present in a single row, with dimensions nearly identical to those of the pterygoid but smaller than those of the vomer.

Palatoquadrate elements

The paired quadrate contacts the squamosal dorsally, quadratojugal laterally, and pterygoid ventromedially (Figs 3, 4). The broad medial surface is likely to have received the distal end of the paroccipital process of the opisthotic. As noted by Dilkes (1998), structures include a large quadrate foramen (formed with quadratojugal) (Figs 3A, 4A) and a flat, transversely oriented articular condyle.

The ectopterygoid is a paired, mediolaterally oriented, hourglass-shaped element (in dorsoventral view), whose enlarged ends form a lateral, abutting contact with the jugal and overlap the pterygoid medially (Figs 3, 4B, 8). The latter contact is largely transverse and involves the pterygoid wing but does not extend to the lateral extremity of that structure. The ectopterygoid narrowly misses the posterior end of the maxillae laterally and palatine medially. The anterior margin is subtly concave where it forms the posterior wall of the suborbital fenestra. The posterior margin is deeply concave where it helps to define the anteroventral wall of the adductor chamber. The paired epipterygoid lies anterior to the braincase and includes a quadrangular base that forms a broad, posteriorly ascending contact with the dorsal process of the pterygoid (Figs 3, 4, 7). The columnar dorsal process lacks bony contacts.

The paired pterygoid was thoroughly described by Dilkes (1998), and our data add few significant details. Contacts include the vomer, palatine, and ectopterygoid anteriorly, the parabasisphenoid and quadrate posteriorly, and the epipterygoid posterodorsally (Figs 3, 4, 8). As preserved, the pterygoids are separated from each other by an elongate midline space, with narrow contacts present anteriorly (adjacent to the caudal ends of the internal choanae) and posteriorly (immediately behind the base of the epipterygoids).

Mandibles

The paired dentary is the largest element of the anterior mandible and is best preserved on the left side, where only the posteroventral corner is missing (the right dentary is represented only by its anterior tip) (Fig. 10). Dentary length constitutes slightly less than half that of the mandible as a whole. Contacts include the splenial anteromedially, angular posteromedially, surangular posteriorly, and coronoid posterodorsally. The posterior margin is deeply bifurcated, forming a prominent posterodorsal process and a posteroventral process. (Fig. 10A). The former tapers to a sharp point, whereas the distal end of the latter process is missing. The dentary is the only tooth-bearing element of the lower jaw, with a single row of 14 teeth (see Discussion). The dentary forms the roof and lateral wall of

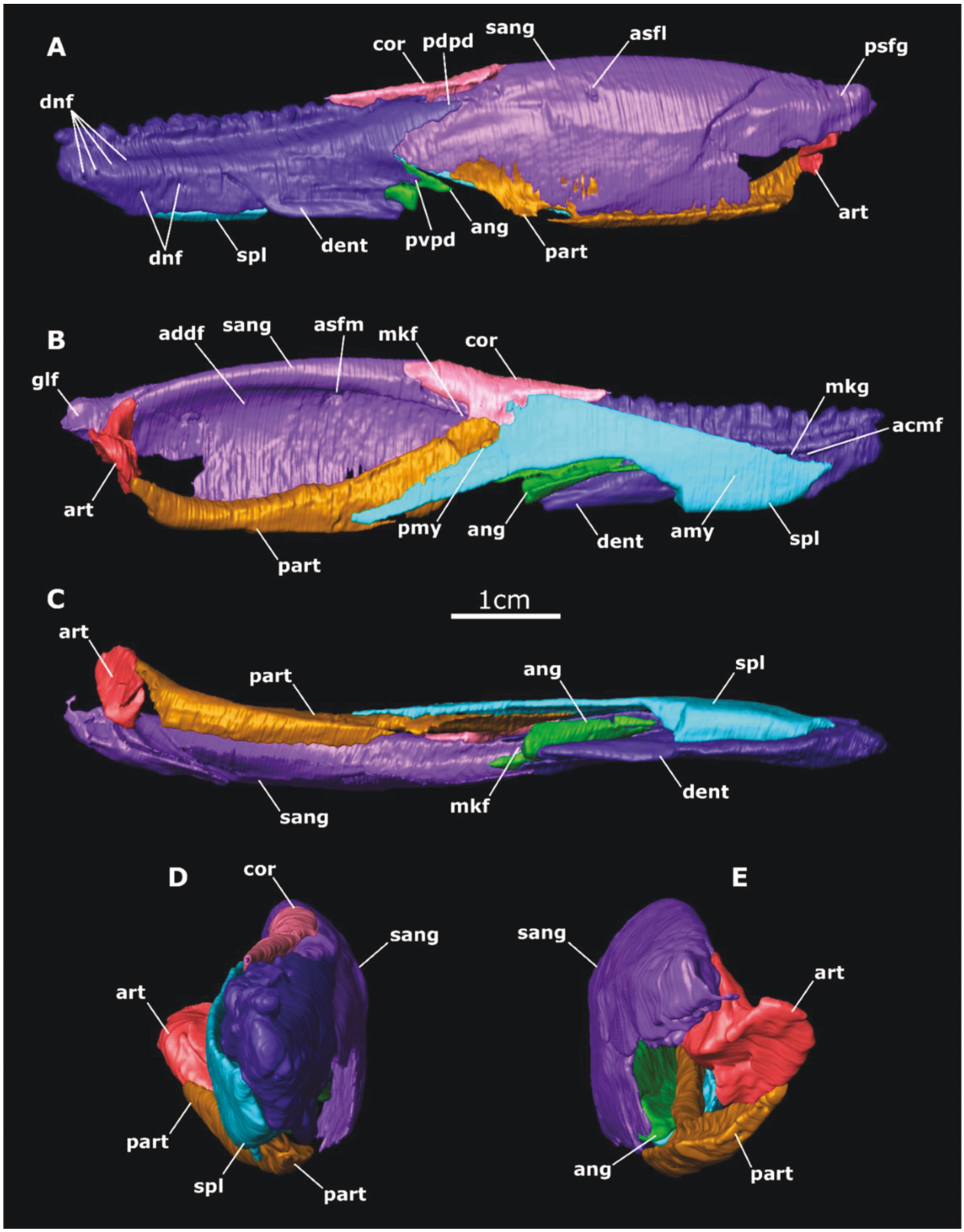

Figure 10. Digitally isolated left mandible of SAM-PK-6536, *Mesosuchus browni*, in: A, lateral; B, medial; C, ventral; D, anterior; and E, posterior views.

the Meckelian canal, which is completed ventrally and laterally by the splenial. The lateral surface of the dentary is pierced by a series of small foramina arranged in two elongate rows (Fig. 10A) and by a smaller number of larger, anterior foramina, all of which communicate internally with the inferior alveolar canal (see Canal section).

Computed tomography reveals that only the anterior end of the left angular is preserved in SAM-PK-6536 (Fig. 10); however, another specimen of *Mesosuchus* preserves the entire element (Dilkes 1998: fig. 8) and forms much of the posteroventral margin of the mandible. The preserved portion lies *in situ*, slotted between the dentary and splenial and contributing to the floor of the Meckelian fossa.

The surangular is an expansive, plate-like element that forms the lateral surface of the mandible in its posterior half (Fig. 10). Contacts include the dentary anteriorly, coronoid anterodorsally, and articular posteromedially. Its medial surface is dominated by an adductor fossa that opens dorsomedially and is completed ventrally by the prearticular. The broadly convex upper margin of the surangular forms the dorsal apex of the mandible, rising to a level above that of the coronoid. The surangular makes a lateral contribution to the glenoid fossa (Fig. 10B). Anterior and posterior surangular foramina pierce the lateral surface of the element to communicate with the adductor fossa medially (Fig. 10A) (see Discussion).

We confirm a tri-radiate coronoid bone composed of anterior, posteroventral, and posterior processes (Fig. 10). The anterior process overlaps the medial surface of the dentary, whereas the posterolateral process contacts the dorsal surface of the prearticular via a concave depression in the latter element. The posterior process overlaps the dorsal surface of the surangular. The concave region between posterior and posterodorsal processes makes a small contribution to the medial wall of the adductor fossa (Fig. 10B). Lack of a distinctive eminence limits coronoid exposure in lateral view.

An incomplete, left articular is present that is likely to represent the anterolateral portion of the element (Fig. 10). This fragment forms a broad suture with the surangular laterally and also contacts the prearticular anteroventrally. The glenoid fossa extends laterally onto the surangular, but otherwise its morphology is too damaged to interpret. A retroarticular process is present in SAM-PK-6536 but is disarticulated from the rest of the skull and was not CT scanned (see Dilkes 1998: fig. 10B).

Computed tomography reveals that much of the material attributed to the left articular by Dilkes (1998) belongs to the left prearticular, which is complete (Fig. 10). Contacts include the coronoid anterodorsally, splenial anteromedially, surangular ventromedially, and articular posteriorly. The prearticular reaches the anteroposterior midpoint of the mandible, forming the extensive ventrolateral wall of the adductor fossa (Fig. 10B). Its splenial contact is pierced by the posterior mylohyoid foramen, which opens internally within the adductor chamber and would probably have transmitted the posterior mylohyoid nerve to innervate the muscular constrictors of the neck and throat (Fig. 10B) (Oelrich 1956).

The left splenial is mostly complete, missing only a portion of its ventral margin (Fig. 10). Contacts include the dentary and prearticular laterally and the coronoid dorsally. Damage to the element probably obscures contact with the angular. Prearticular contact is via a long, finger-like posterior process. There is no rugosity indicating a splenial contribution to the mandibular symphysis. The mentonian process is weakly developed, leaving the splenial barely exposed in lateral view. The splenial forms the medial and ventral walls of the Meckelian canal and fossa and is pierced by anterior (*contra* Dilkes 1998) and posterior mylohyoid foramina (the latter completed by the prearticular) (Fig. 10B). Both openings communicate with the Meckelian canal. CT data reveal a short canal opening laterally and posteriorly via short secondary canals. These are likely to have conveyed cutaneous branches of the inferior alveolar nerve (V3) (Oelrich 1956).

Neurovascular canals

Given the paucity of high-quality CT data for stem archosaurs, we take this opportunity to detail the morphology of selected canal systems. The superior alveolar canal (SAC) runs the horizontal length of the maxilla and includes a single, large anterior maxillary foramen (AMF) located at the premaxilla–maxilla suture, multiple minor lateral canals that exit onto the lateral face of the maxilla (LACs), a rostral posteromedial foramen (RPMF), and a caudal posteromedial foramen (CPMF) (Fig. 11A–D). These observations align closely with those for the stem reptile *Orovenator mayorum* Reisz *et al.*, 2011, stem archosaur *Prolacerta broomi* (Benoit *et al.* 2021), and stem lepidosaur *Marmoretta oxoniensis* Evans, 1991 (Griffiths *et al.* 2021), suggesting that this morphology is both plesiomorphic for reptiles and highly conserved across the base of the radiation of the group. A similar large anterior foramen of the SAC is described in *Rhynchosaurus articeps* (Benton 1990) and *Hyperodapedon gordoni* (Benton, 1989). Multiple lateral foramina and a single posterior foramen are also recorded in the latter taxon.

The RPMF in *Mesosuchus* is aligned with a groove in the maxillary process of the palatine that in extant lepidosaurs transports the anteriorly coursing maxillary artery, vein, and nerve following their traversal of the suborbital foramen and prior to their entry into the superior alveolar canal (Figs 5, 7, 8) (O'Donoghue 1921; Oelrich 1956, Porter and Witmer 2015). This bony signature appears to be lacking in the crocodilian and avian palate. In extant turtles, three major posteromedial openings communicate with the SAC, transporting branches of the maxillary nerve, artery, and vein (Albrecht 1976, Bever 2009). The SAC continues for a short distance within the maxilla before giving off a narrow caudal canal that courses almost the entire length of the posterior process of the maxilla to emerge via the CPMF (Fig. 11A–D). This branching pattern is consistent with that figured in *Prolacerta broomi*, *Orovenator mayorum* (Benoit *et al.* 2021: fig. 1), *Ctenosaura pectinata* Wiegmann, 1828 (Oelrich 1956), and *Iguana iguana* Linneaus, 1758 (Porter and Witmer 2015: fig. 3), although the latter two taxa appear to lack a CPMF, and the caudal canal ends blindly within the posterior process of the maxilla. We could find no reference to a caudal branch of the alveolar canal in turtles. There appears to be no evidence of either a RPMF or a CPMF in any tanystropheid or stem archosaur crownward of *Prolacerta broomi*, although we expect that this is an artefact of scan and/or preservation quality and do not suggest that their maxillae lacked neurovascular excavation. Given the communication of this canal with the SAC proper, it is likely to have contained branches of the maxillary nerve, artery, and vein serving the superficial tissues of the posterior alveolar margin, as in *Ctenosaura* (Oelrich 1956) and *Iguana* (Porter and Witmer 2015).

A large number of small, lateral canals (LACs) are distributed along the length of the SAC (Fig. 11A, B) and would have conveyed sensory innervation and blood to the surface of

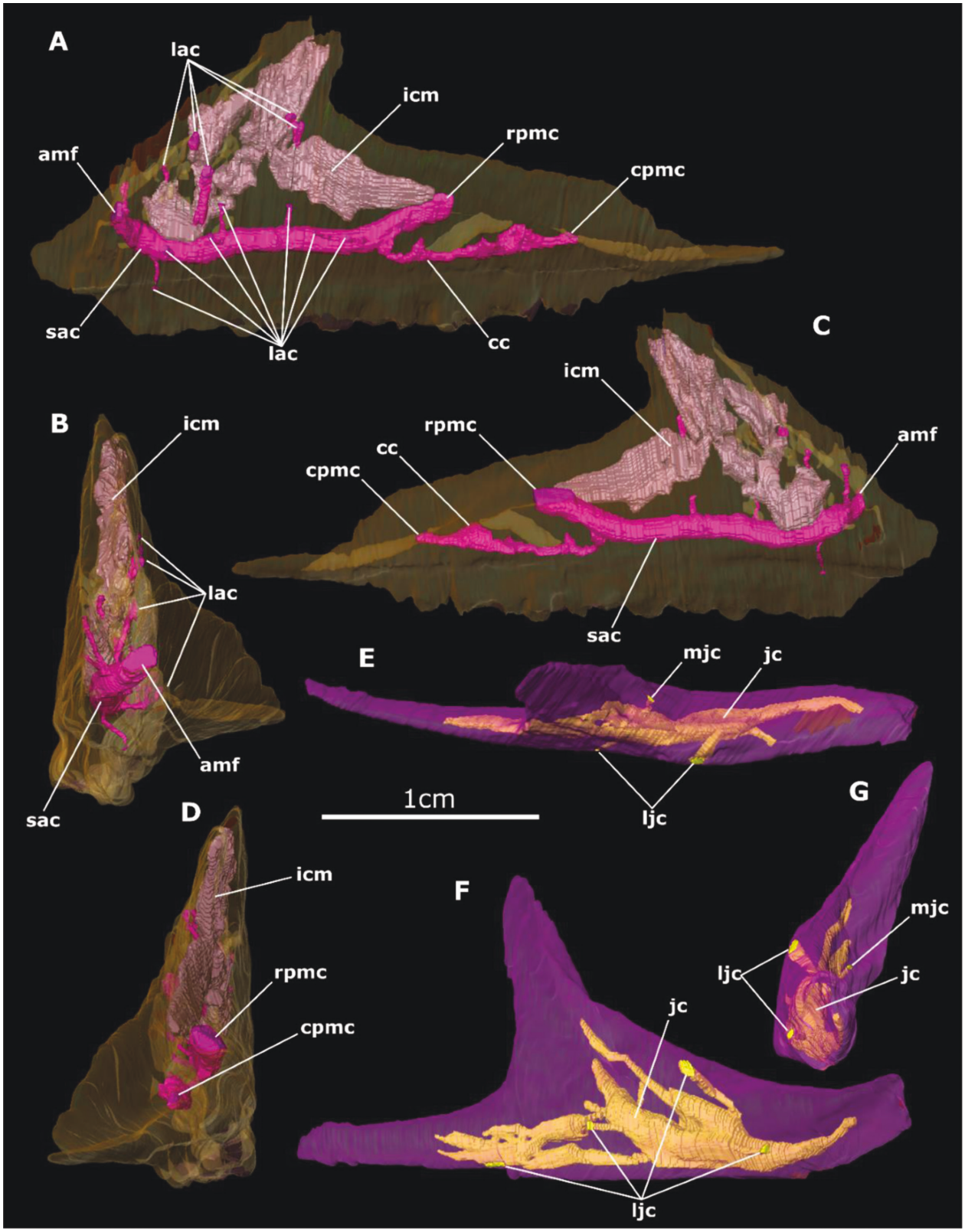

Figure 11. Internal anatomy of the left maxilla and right jugal of SAM-PK-6536, *Mesosuchus browni*: A, left maxilla in lateral view; B, left maxilla in anterior view; C, left maxilla in medial view; D, left maxilla in posterior view; E, right jugal in dorsal view; F, right jugal in lateral view; and G, right jugal in anterior view.

the snout (Porter and Witmer 2015, 2020, Porter *et al.* 2016, Bouabdellah *et al.* 2022). The density of these foramina was used as evidence of a rhamphotheca in edentulous pan-archosaurs (Wynd *et al.* 2020). Interestingly, the 'beaked' forms of deeply nested rhynchosaurs were deemed to lack these keratinous sheaths based on the apparent absence of densely packed LACs

(Sill 1971, Langer and Schultz 2000). Given the number of these openings in *Mesosuchus*, we suspect that CT data for 'beaked' rhynchosaurs will boost the evidence for their possession of a maxillary rhamphotheca.

The roof of the distal end of the SAC is excavated anteriorly by a cavity secondarily linked to a series of chambers that extend throughout the maxilla (Fig. 11A–D; see Discussion). Several of these chambers give off minor canals that emerge onto the lateral surface of the maxilla as LACs. Given the communication of these spaces with the SAC, they are likely to have transported neurovascular bundles from the maxillary artery, vein, and nerve (V2).

The distal exit of the SAC takes the form of an anteriorly opening foramen that is situated almost within the maxilla–premaxilla suture (Figs 3, 5, 11). It can be differentiated from the LACs by its relative size and by the anteriorly facing orientation of its aperture. A foramen in this location is identified in the stem archosaurs *Prolacerta broomi* and *Proterosuchus fergusi* Broom, 1903 (Welman 1998) and is expressed sporadically amongst stem crocodylian taxa (for an expanded discussion, see Nesbitt 2011). This feature is present in extant lepidosaurs (O'Donoghue 1921, Oelrich 1956, Porter and Witmer 2015) and testudines (Rollot *et al.* 2024) and marks the point at which the maxillary neurovascular bundle emerges from the SAC to innervate and supply the cutaneous tissue of the external nostril.

The jugal of SAM-PK-6536 houses a canal that extends for nearly the entire rostrocaudal length of the bone (Fig. 11E–G). A medial opening into this canal is visible in the right jugal only and lies within a shallow concavity between the posterior point of divergence of the dorsal and posterior processes. The canal itself communicates with the lateral surface of the jugal via a series of openings, which are also present in the early rhynchosaurs *Howesia browni* and *Eohyosaurus wolvaardti* and in the rhynchosaurids *Langeronyx brodiei* and *Hyperodapedon gordoni* (Benton 1983). In *Hyperodapedon gordoni*, a large lateral foramen is referred to as a 'major vessel opening' (Benton 1983: p. 620), but its internal course is not described. There are no distinctively large lateral foramina in SAM-PK-6536, although a smaller foramen does occupy the homologous position of the *Hyperodapedon gordoni* opening in both left and right elements, immediately anterior to the divergence of the dorsal and posterior processes (Benton 1983). CT data of *Hyperodapedon sanjuanenis* do not reveal any internal structure within the jugal. A jugal canal is not reported in any stem reptiles (e.g. *Youngina capensis*) or stem testudines [e.g. *Eunotosaurus africanus* or *Eubaena cephalica* Hay, 1904 (Rollot *et al.* 2018)]. We confirmed the presence of a jugal canal in *Alligator mississippiensis* Daudin, 1801 and *Sphenodon punctatus* Gray, 1842 (see also Osawa 1898) that is accompanied by a medial foramen similar to that of SAM-PK-6536. The contents of this canal are not reported in *Sphenodon*, although in *Alligator mississippiensis* the jugal receives rostral and caudal internal branches of the palatomaxillary artery as it passes medially (Porter *et al.* 2016). The *Alligator mississippiensis* jugal is also perforated by lateral fibres of the maxillary nerve (V2) that provide cutaneous innervation to the cheek region (Lessner and Holliday 2022a, Lessner *et al.* 2022a). In crown turtles, a minor branch of the supraorbital artery perforates the jugal medially, but it is unclear whether this leads to a well-developed canal (Albrecht 1976). In squamates, the jugal is not perforated by any neurovasculature (Porter and Witmer 2015).

The inferior alveolar canal of the lower jaw passes through the dentary, lateral to Meckel's canal (Fig. 12A–C). This structure undoubtedly conveyed the inferior alveolar nerve and branches of the intramandibular artery and vein to the lower dentition and neighbouring soft tissues, as in extant reptiles (Evans 2008, Kawabe and Hattori 2022, Lessner and Holliday 2022a, b, Evers *et al.* 2023, Crole and Soley 2016). The neurovasculature would have entered the canal through the medial posterior alveolar foramen, positioned near the tail end of the Meckelian fossa. Small, lateral canals populate the length of the primary canal in a pattern that is assuredly plesiomorphic (O'Donoghue 1921, Bhatia 1929, King and McLelland 1975, Porter and Witmer 2015, 2016, Porter *et al.* 2016, Evers *et al.* 2023). The density of these lateral canals does not match the derived state of crocodilians, which make use of densely packed sensory fibres to facilitate their specialized mode of aquatic sensory perception (Leitch and Catania 2012). The relative number and density of lateral mandibular foramina matches that observed in 'beaked' rhynchosaurs (e.g. *Hyperodapedon gordoni*). The primary canal bifurcates anteriorly into a minor branch that exits onto the anterior tip of the dentary (as the rostral-most opening of the system) and a larger branch that turns medially to exit immediately dorsal to the anterior tip of the splenial (Fig. 12B, C).

To our knowledge, the canal passing mediolaterally through the anterior splenial, as in SAM-PK-6536, has not been described previously in the stem archosaur literature (Fig. 12D–F). The presence of a foramen in the medial surface of the element, however, is observed in both *Rhynchosaurus articeps* (Benton 1990: fig. 8) and *Hyperodapedon gordoni* (Benton 1983: fig. 13). We interpret this space as having conveyed the mylohyoid branch of V3, as in *Sphenodon* (Benton 1983), *Ctenosaura* (Oelrich 1956), and crocodylians (Miall 1878). Thus, we homologize its external opening with the anterior mylohyoid foramen of other reptiles (e.g. Evans 2008, Brusatte *et al.* 2009, von Baczko and Desojo 2016).

A pair of foramina perforate the lateral surface of the surangular: the anterior and posterior surangular foramina (Fig. 10A). The anterior foramen opens around midway along the length of the element within an internal canal that passes horizontally before emerging into the adductor fossa (Fig. 10B). A similar anterior foramen is present in *Prolacerta broomi* and *Euparkeria capensis*. The posterior surangular foramen lies ventral to the posterodorsal corner of the element, as in other rhynchosaurs (e.g. Butler *et al.* 2015, Gentil and Ezcurra 2022) and non-rhynchosaurian stem archosaurs (e.g. Welman 1998, Modesto and Sues 2004, Sookias *et al.* 2020). A posterior surangular foramen is also present in extant squamates (Oelrich 1956, Klembara *et al.* 2014) and the stem rhynchocephalian *Gephyrosaurus bridensis* Evans, 1980 (Evans 1980). In turtles, foramen auriculotemporalis also opens medially onto the surangular (Gaffney 1979, Evers *et al.* 2023). Interpretations regarding the contents of the anterior and posterior surangular foramina are rare, although based on their contents in crown testudines and squamates, these foramina might have contained cutaneous branches of the inferior alveolar nerve (V3) and mandibular artery (Oelrich 1956, Evers *et al.* 2023).

Phylogenetic analysis

Our re-scoring of *Mesosuchus* in the matrix of Scheyer (2020) modified previous scorings for 24 published characters; these include: 24 (0 to 1), 25 (2 to 1), 29 (1 to 0), 76 (0 to 1), 93 (0 to

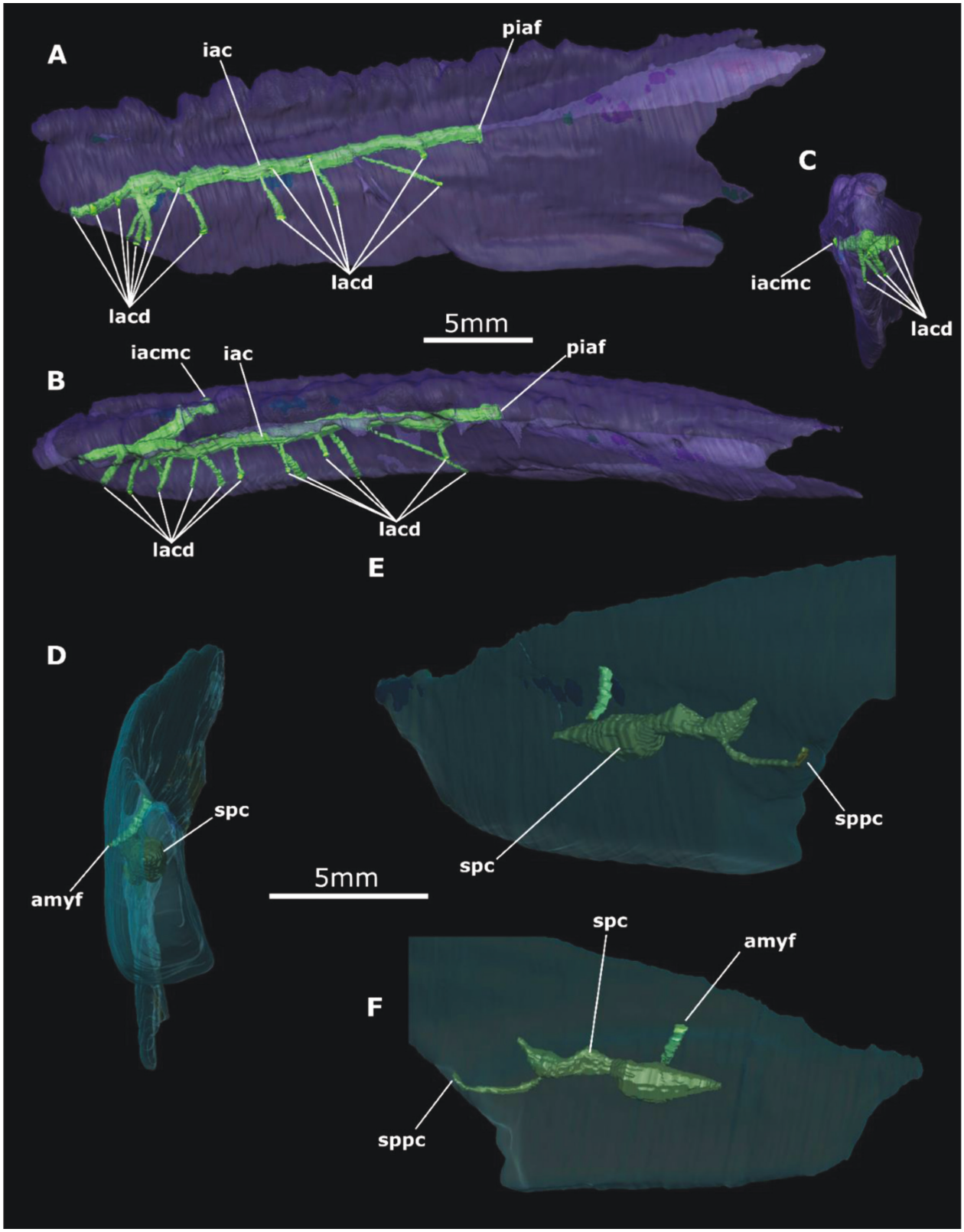

Figure 12. Internal anatomy of left dentary and splenial of SAM-PK-6536, *Mesosuchus browni*: A, left dentary in lateral view; B, left dentary in dorsal view; C, left dentary in anterior view; D, left splenial in anterior view; E, left splenial in posterolateral view; F, left splenial in medial view.

1), 115 (0 to 1), 120 (? to 0), 121 (? to 0), 131 (0 to 1), 137 (0 to 1), 161 (1 to 0), 183 (0 to 1), 191 (0 to 1), 206 (1 to 0), 266 (? to 0), 268 (0 to 1), 270 (? to 0), 279 (2 to 0), 280 (1 to 0), 281 (? to 0), 287 (1 to 0), 309 (? to 0), 614 (? to 1), and 636 (0 to 1). Our analysis found 27 most parsimonious trees with a tree length of 3872, consistency index of 0.238, and retention index of .643.

Our strict consensus tree is nearly identical to that of Scheyer (2020), in terms of topology and Bremer support (Fig. 13). Amongst Rhynchosauria, only *Ammorhynchus navajoi* Nesbitt and Whatley, 2004 (Nesbitt *et al.* 2004) changes position and is included within a polytomy consisting of the Chañares rhynchosaur, *Brasinorhynchus mariantensis* Schults *et al.*, 2016 (Schultz *et*

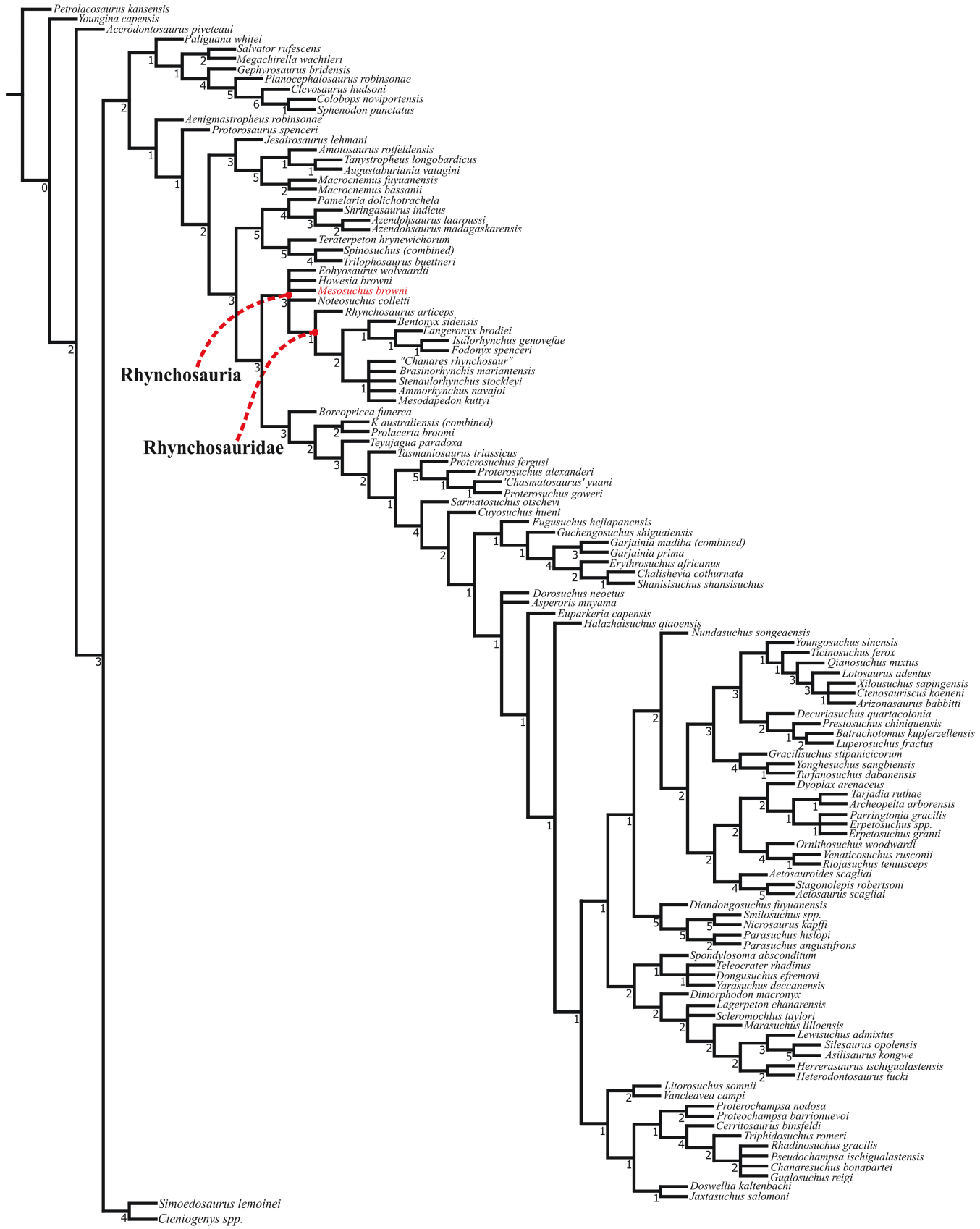

Figure 13. Strict consensus tree calculated from our re-analysis of the character matrix constructed by Scheyer *et al.* (2020) with adjusted scorings for *Mesosuchus browni*. *Mesosuchus browni* is presented in red text, and the clades Rhynchosauria and Rhynchosauridae are labelled.

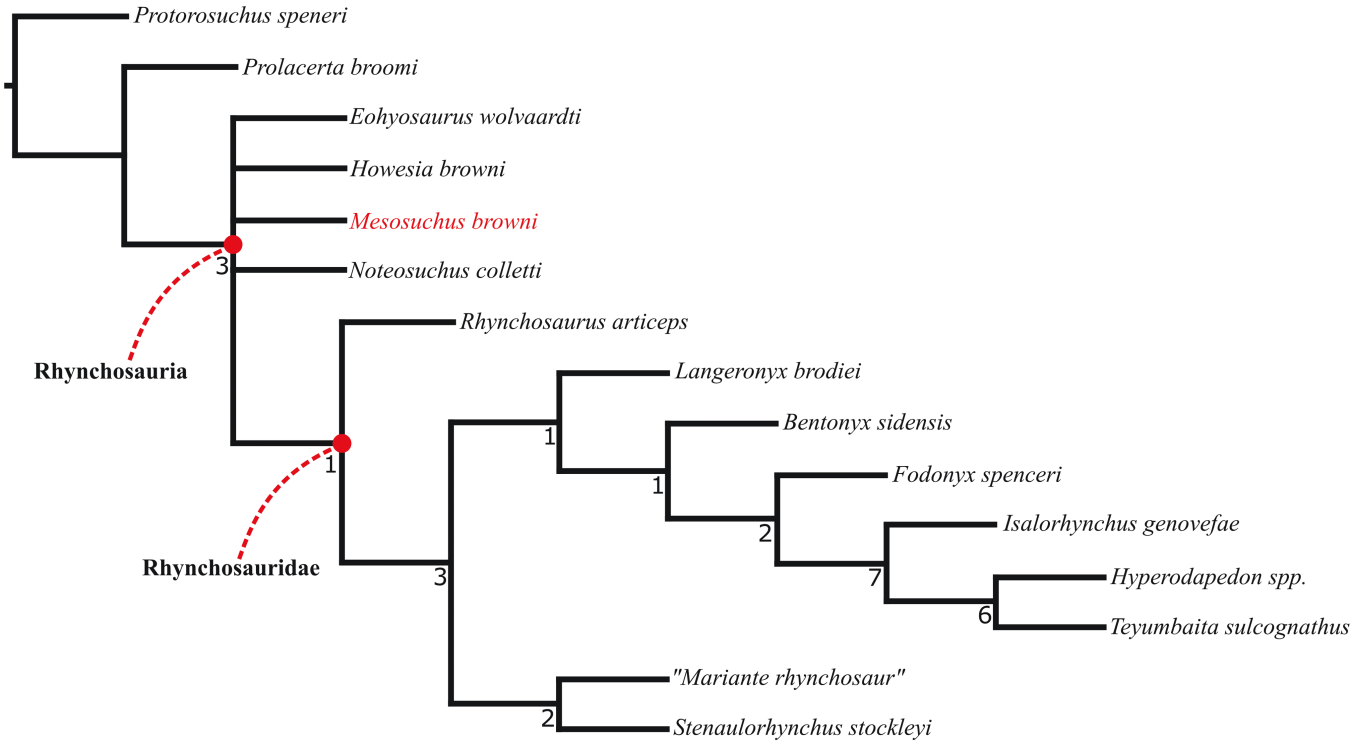

Figure 14. Strict consensus tree calculated from our re-analysis of the character matrix constructed by Ezcurra *et al.* (2016), with adjusted scorings for *Mesosuchus browni*. *Mesosuchus browni* is presented in red text, and the clades Rhynchosauria and Rhynchosauridae are labelled.

al. 2016), *Stenaulorhynchus*, and *Mesodepedon kuttyi* Chatterjee, 1980.

Our re-scoring of *Mesosuchus* in the matrix of Ezcurra *et al* (2016) modified previous scorings for six published characters; these include: 11 (0 to 1), 16 (? to 0), 41 (0 to 1), 44 (0 to 1), 69 (? to 1), and 73 (0 to 1). Our 'traditional search' analysis found two most parsimonious trees with a tree length of 150 (two steps higher than in the study by Ezcurra *et al.* 2016), a consistency index of .687, and a retention index of .766. Our strict consensus tree matches exactly the topology of Ezcurra *et al.* (2016) (Fig. 14). Apomorphies that diagnose (i) Rhynchosauria + crownward Pan-Archosauria, (ii) Rhynchosauria, and (iii) *Mesosuchus* itself (i.e. autapomorphies) are listed for both analyses as Supporting Information (Appendix S1).

DISCUSSION

Vomeronasal system and septomaxilla

Vomerolfaction is a chemosensory system (VNS) capable of processing macromolecules, such as pheromones (Bertmar 1981). Its evolutionary origins can be traced to the osteichthyan stem lineage (Grus and Zhang 2006, González *et al.* 2010, Nakamuta *et al.* 2012); however, it is within Tetrapoda, and most notably Amniota, that the VNS reaches its greatest degree of functional and structural complexity. This development is perhaps best exemplified among the squamate reptiles, in which the VNS is implicated in a wide range of sophisticated tasks that include conspecific recognition (Labra and Niemeyer 1999), reproductive selection (López and Martín 2004), and prey tracking (Rehorek *et al.* 2000a, b, Baeckens *et al.* 2017).

The anatomy and physiology of the amniote VNS is highly similar to that of primary olfaction (Eisthen 1992). It includes a parasagittal pair of vomeronasal organs (VNOs, sometimes called Jacobson's organs) located adjacent to the external nares. These organs include a specialized epithelium that collects sensory input and conveys that information to a dedicated accessory lobe of the telencephalon via the vomeronasal nerve (cranial nerve I) (Halpern 1987). Structural support of this system extends to modifications of the primary palate. For example, the mammalian VNO lies within a dedicated diverticulum of the nasal cavity and is connected to the oral cavity via a nasopalatine duct (Bertmar 1981). In extant reptiles that retain the VNO (i.e. lepidosaurs), it is usually housed within a cavity of the anterior rostrum that is bounded by the septomaxilla dorsally and vomer ventrally. This cavity is sometimes referred to as cupola Jacobsoni (Rieppel *et al.* 2008) or Jacobson's chamber (Klembara *et al.* 2014). The reptile VNO tends to lie near the distal opening of the nasolacrimal duct and its bony canal. The exact functional relationship with the nasolacrimal system remains poorly understood, but the VNO is likely to receive secretions from the Harderian gland of the orbit through this pathway (Hillenius and Rehorek 2005, Rehorek 1997, 1999).

The generally conserved nature of the VNS in Pan-Mammalia coupled with its prominent status within the sensory repertoire of lepidosaurs (Bellairs and Boyd 1947, 1950, Cooper 1996) supports its presence along the reptile stem lineage. The crown clades of turtles, crocodylians, and birds, however, each exhibit a reduced VNS. Extant turtles possess a vomeronasal nerve (Cotter 1917) and accessory olfactory lobe (Crosby and Humphrey 1939); a VNO is present, but it is relegated to a small patch of epithelia in the posteroventral floor of the nasal passage

(Schwenk and Thewissen 2008, Kondoh *et al.* 2021) and is not integrated with the nasolacrimal apparatus, which is entirely absent (Bellairs and Boyd 1947, Baccari *et al.* 1992). Adult birds and crocodiles all lack the VNO (Parsons 1959), vomeronasal nerve (Wenzel 1987), and accessory olfactory bulb (Crosby and Humphrey 1939, Wenzel 1987). VNO anlagen apparently form in both groups, but fail to develop into an adult phenotype (Meek 1893, Slabý 1955, Parsons 1959, Romanoff 1960). The presence of these anlagen is intriguing because it indicates that some proportion of the developmental network (Davidson 2006, Wagner 2007) patterning the VNS was conserved over the entirety of the avian, crocodilian, and archosaurian stem lineages, currently estimated at ~130, 150, and 25 Myr, respectively (Oaks 2011, Jetz 2012). VNS comparisons amongst extant taxa justify the inference that an initial reduction of VNS morphogenesis is a synapomorphy of Archelosauria (the crown clade defined by the exclusive split that produced Pan-Testudines and Pan-Archosauria), followed by a further reduction somewhere along the archosaur stem lineage. Testing the secondary homology of archelosaur reductions requires the use of bony correlates of the VNS to determine whether stem representatives (i.e. fossils) of archelosaurian crown clades retained fully developed forms of the system.

Fossil discoveries over the last 20 years have significantly increased our understanding of the turtle stem lineage (Li *et al.* 2009, 2018, Lyson *et al.* 2010, Bever *et al.* 2015, Schoch and Sues 2015). Among these studies, the only available CT-based analysis is that of Bever *et al.* (2015), which did not produce skeletal evidence of a VNS, such as a septomaxilla (see below), in the earliest and most controversial of the putative stem turtles, *Eunotosaurus africanus*. Although the palate of *Eunotosaurus africanus* is far from perfect, absence of what would be a plesiomorphically elaborate VNS is also lacking in the more extensively preserved and described crownward stem turtle, *Proganochelys quenstedti* Baur, 1887 (Gaffney 1990). These findings thus suggest that a reduced form of the turtle VNS might well characterize the entirety of its long stem lineage and might ultimately find its origin along the archelosaur stem.

The problem with this hypothesis of archelosaur reduction is that with our description of *Mesosuchus*, we now have extensive skeletal evidence of a structurally complex and elaborate VNS in a stem archosaur. The wide space in the anterior palate of SAM-PK-6536 circumscribed by the septomaxilla (dorsally) and vomer (ventrally) is positionally homologous to the squamate Jacobson's chamber (Fig. 9). Its posteroventral continuity with the choanae would have facilitated sensory input via the oral cavity, as in the 'palaeochoanate' condition of *Sphenodon* and iguanians (Rieppel *et al.* 2008). Presence of a VNS in *Mesosuchus* is also supported by the spatial relationships of its nasolacrimal canal. In squamates and mammals, the nasolacrimal canal passes from the orbital rim directly into the nasal cavity and continues in a cartilaginous form to connect directly with Jacobson's chamber (Kaczmarek *et al.* 2020). The finding that the nasolacrimal canal of SAM-PK-6536 has an anterior opening into the nasal cavity (Fig. 5A) that lies in close proximity to a pair of posterior openings into Jacobson's chamber is congruent with a VNS configuration. We interpret one of these two openings to have conveyed the distal length of the nasolacrimal duct, whereas the other is likely to have housed a neurovascular bundle composed of branches of the maxillary artery and medial ethmoidal nerve, as in squamates (e.g. Bellairs 1949, Oelrich 1956). In extant archelosaurs that have reduced or lost vomerolfaction, the nasolacrimal duct is either absent (Testudines; Rehorek *et al.* 2000a, b) or opens more posteriorly, away from the region that would, plesiomorphically, have housed a VNO (Archosauria; Witmer 1995, Cerio and Witmer 2023, Rehorek *et al.* 2022).

Additional evidence for a VNS in *Mesosuchus* is derived from elements of the skull roof. We interpret the deep (internal) concavities of the lacrimal, prefrontal, and frontal as having housed expanded olfactory and accessory olfactory bulbs of the telencephalon, making them bony signatures of a well-developed VNS (Figs 5, 6). In extant lepidosaurs and, to a lesser degree, turtles, the olfactory bulb is regionalized into a large and ventrally positioned main olfactory bulb and a smaller accessory olfactory bulb that usually lies on the dorsal surface of the main olfactory bulb (Armstrong *et al.* 1953, Lohman and Smeets 1993), in a pattern congruent with the concavities of the *Mesosuchus* skull roof. An obvious groove for the olfactory tract in the frontals of *Mesosuchus* is shared with other stem archosaurs (e.g. *Macrocnemus bassanii*). In *Mesosuchus*, this groove widens anteriorly to form a deep oval concavity that, in turn, communicates with an even deeper excavation of the anterolateral portion of the frontal and the medial surfaces of both the prefrontal and the lacrimal. Thus, there are impressions of two spatially segregated lobes in the olfactory region of the endocranial space.

Given the apparent correlation between VNS reduction and simplification of the anterior palate, including loss of the septomaxilla, it is possible that VNS tissues and the septomaxilla share a level of developmental modularity and that the loss of one constituent results in the loss or simplification of the other. In addition to *Mesosuchus*, a septomaxilla is reported in a number of stem archosaurs, with the phylogenetically earliest example being the allokotosaur *Trilophosaurus buettneri* Case, 1928; however, published descriptions lack morphological detail (Gregory 1945), and one source claims that it is absent in this taxon (Parks 1969). Among rhynchosaurs, the septomaxilla is also known in *Teyumbaita sulcognathus* (Montefeltro *et al.* 2010), *Hyperodapedon marienensis* Tupi-Caldas, 1933 (Langer and Schultz 2000), and *Hyperodapedon sanjuanensis*. Although the septomaxilla remains a dominant element in the anterior palate of these rhynchosaurids, it is a flat plate that lacks the structural complexity of the *Mesosuchus* element. The plate is robustly sutured to the vomer posteriorly and the maxillae laterally. In this configuration, the element is an integrated component of the horizontally oriented bony palate and does not circumscribe a Jacobson's chamber. Given these features, we hypothesize that the VNS was reduced or even lost as a derived transformation within the rhynchosaur radiation and in parallel with that of other reptile clades.

Pan-archosaurs positioned crownward of rhynchosaurs and possessing a septomaxilla include *Prolacerta broomi* and both *Proterosuchus fergusi* and *Proterosuchus goweri* Ezcurra and Butler, 2015 (Ezcurra and Butler 2015, Ezcurra 2016). Morphological details of this element in these taxa are difficult to discern; the available CT data for the former lack the necessary resolution in this region, whereas the preservation of the snout in the latter two is relatively poor. The majority of other stem archosaurs lack reported septomaxillae, which is difficult to interpret

biologically. The delicate nature of this element inevitably incurs some measure of taphonomic modification. Adding to this the combination of its internalized position and the current scarcity of relevant CT datasets, we conclude that we are dealing with a highly conserved stem archosaur septomaxilla that is woefully under-sampled. Nevertheless, the failure of CT data to reveal septomaxillae in *Macrocnemus bassanii*, *Tanystropheus hydroides* Spiekman *et al.*, 2020 (Spiekman *et al.* 2020), *Tanystropheus longobardicus* Bassani, 1886 (Nosotti 2007), and *Euparkeria capensis* should give pause to the presumption that the phylogenetically complex distribution of this bone, and the VNS it supports, lacks biological meaning.

The late Triassic phytosaurs expand the arc of this discussion. Many phytosaur taxa possess anterior ossifications of the anterior snout that may contribute to the nasal septum and have been named 'septomaxillae' (e.g. Datta *et al.* 2021; Heckert *et al.* 2021). The problem is that these phytosaur elements are plate-like structures of the cavity roof rather than the cavity floor (see Stocker 2010). Such dorsal displacement, although possible, would also disrupt any spatial or developmental relationship between the septomaxilla and a VNS as we currently understand it. These phytosaur elements are certainly far removed from the oral cavity and nasolacrimal duct. It is thus probable that the phytosaur bones lack an exclusive identity (i.e. are non-homologous) with the tetrapod septomaxillae (Sereno 1991, Senter 2002, Stocker 2010, Nesbitt 2011), although both elements might be the product of a shared, derived propensity for ossification in the anterior snout. Historically, phytosaurs were considered an early radiation of stem crocodylians (e.g. Gauthier 1984, Benton and Clark 1988, Brusatte *et al.* 2010), whereas more recent work pushes them into a stem position slightly outside the crown (e.g. Nesbitt 2011, Sookias *et al.* 2014, Ezcurra 2016). Regardless of whether their septomaxillae are homologous to that of *Mesosuchus* or not, a stem position for phytosaurs constitutes evidence that any integration between a complex septomaxilla with a well-developed VNS was lost long before the origin of the archosaur crown clade.

Combining the phylogenetic distribution of the VNS and its anatomical components with the persistence of an albeit truncated developmental signature in crown archosaurs suggests that this system enjoys widespread conservation in terms of its developmental/molecular foundation, if not in its functional identity. Such conservation is seemingly amenable to numerous, parallel acquisitions of the functional, adult phenotype. The dynamics responsible for maintaining this potential and for shifting between the suppressed and expressed conditions can and should be investigated with developmental and genomic data. Sequences specific to the VNS have yet to receive detailed study in reptiles, although there is some suggestion that they are closely tied to the primary olfactory regions of the genome and are not entirely functionally independent (Suárez *et al.* 2012). These genes evolve at least one order of magnitude more rapidly than any other protein-coding genes and are highly responsive to environmental chemical conditions (Yohe *et al.* 2020). This increased rate might be responsible, at least in part, for the erratic patterns of gain and loss of the septomaxilla and, potentially, the VNS on the archosaur stem lineage.

If *Mesosuchus* did possess a fully functioning VNS, what conclusions might be drawn regarding its behavioural ecology? It was shown that a fossorial ecology bears some correlation with a hypertrophied VNS (Halpern 1987, Cooper 1996). It was also argued that fossoriality was a relatively common behavioural strategy in the Permo-Triassic vertebrate communities of the Karoo sequence and might even have heightened fitness in relationship to the Permian–Triassic extinction event (Botha 2003, Smith and Botha 2009, Lyson *et al.* 2016). It is certainly possible that *Mesosuchus* was fossorial to some degree (i.e. we cannot currently reject that as a hypothesis). Without direct evidence of burrowing or clear postcranial adaptations for digging, however, a presumed VNS based on an as-yet-to-be established developmental correlation with the morphology of the primary palate is hardly convincing. The wide range of behaviours that the VNS supports among extant squamates complicates any attempt to establish tight, predictive correlations for behaviour in the fossil record. This point has broader implications than for interpreting *Mesosuchus*. For example, many extant lineages that underwent a secondary aquatic transition exhibit a reduction of such structures (Kishida *et al.* 2007, Korsching 2016, Lu *et al.* 2016), which could have implications for the apparent loss of the septomaxilla (and any associated VNS) in the secondarily aquatic Tanystropheidae (Sennikov 2011, De Oliveira *et al.* 2018, Spiekman *et al.* 2020). Evidence for the presence of VNOs in sauropterygians (Buchy *et al.* 2006, Voeten *et al.* 2018), mosasaurs (Lingham-Soliar 1995, Schulp *et al.* 2005), and in the marine-adapted extant iguanas of the Galápagos (Paparella and Caldwell, 2022) implies that this correlation is not strictly applicable to all lineages.

Homology of elements P

To our knowledge, the paired ossifications of SAM-PK-6536 that lie directly anterior to the vomers within the primary palate are unique among reptiles. Their bilateral symmetry, in both shape and position, make them unlikely to be products of damage, either to the vomer or to the nearby premaxilla. It is possible that elements P, as a paired ossification centre, is not unique but that its true phylogenetic distribution is obscured by a secondary integration with the vomer. Ossification studies of the amniote vomer indicate a single, posterior centre that expands rostrally as morphogenesis unfolds. This pattern includes lineages that retain the vomer as a paired, adult element (e.g. Ollonen *et al.* 2018) and those where paired centres fuse to produce a single midline bone [i.e. mammals (Terry 1909), turtles (Rieppel 1993a), and crocodylians (Rieppel 1993b)]. It is notable, however, that these studies tend to examine only late-stage morphogenesis, leaving open the possibility of more complex dynamics in early ontogeny. Studies concentrating on pre-ossification mesenchymal patterning in this region are rare, although two studies reported that both the septomaxilla and the vomer initiate ossification at multiple condensations (Polachowski and Werneburg 2013, Sheverdyukova 2019). Whether such complex patterns of early development characterize the reptile palate outside of snakes is, as yet, unknown. If such a pattern underlies the morphology of *Mesosuchus*, elements P might represent a paired centre that retained its identity through morphogenesis (thus becoming an individuated bone) rather than being subsumed with an inclusive vomer.

Antorbital pneumatization

The neurocranial and antorbital (facial) regions of the crown archosaur are highly pneumatized, supporting the inference

that the origin(s) of these integrations lie somewhere along the archosaur stem lineage (Witmer and Ridgley 2009, Dufeau and Witmer 2015). An argument was made recently that the neurocranium of rhynchosaurs, including but not exclusive to *Mesosuchus*, is pneumatized (Sobral and Müller 2019). This neurocranial signature was subsequently extended even deeper along the archosaur stem to the allokotosaur *Trilophosaurus* (Wilson *et al.* 2022). We add to this scenario an interpretation that *Mesosuchus* also possessed antorbital pneumatization as evidenced by the highly excavated internal morphology of the maxillae. These elements contain an extensive system of connected, bilaterally symmetrical cavities that can be distinguished readily from the network of air cells comprising adjacent cancellous bone. The cavities communicate anteriorly with the superior alveolar canal and laterally with external foramina. In this anterior morphology, the *Mesosuchus* condition is not entirely dissimilar from that described for the stem reptile *Orovenator* and for the crownward stem archosaur *Prolacerta broomi*, neither of which is interpreted as pneumatic (Benoit *et al.* 2021). The distinction of the *Mesosuchus* condition is in the degree to which internal cavities fill the maxillae, extending throughout both the posterior and dorsal processes.

It is difficult when chasing the stem origin of an important crown feature to be conservative in one's assessments of homology, while at the same time resisting the proclivity to impose a crown-level development as a requirement for identity. This dialectic was discussed by Wilson *et al.* (2022) as it applies to pneumatization, and thus need not be repeated here. We propose that expanded, paranasal diverticula (Witmer 1995, 1997) were in place along the archosaur stem prior to the divergence of rhynchosaurs. The initial invasion of these respiratory epithelia into the facial skeleton was restricted to the maxilla, which they entered through pre-existing neurovascular channels associated with the superior alveolar canal and maxillary nerve (V2). If the anatomy is correctly interpreted, then the absence of antorbital pneumatization in *Prolacerta broomi* constitutes an accelerated versus delayed transformation (ACCTRAN–DELTRAN) problem (Maddison 1994), where either the antorbital pneumaticity of *Mesosuchus* and later pan-archosaurs evolved in parallel and thus lacks secondary homology, or the apneumatic nature of *Prolacerta broomi* is a reversal. Future sampling should resolve this ambiguity, although it is possible that the early history of this complex involved a conservation of paranasal sinuses whose varying levels of relative expansion produced an even more incongruous pattern of bony invasions than currently appreciated.

Implications for rhynchosaurian dental evolution

Rhynchosaurs exhibit a derived form of tooth development and implantation that differs from other stem archosaur clades. Unlike the plesiomorphic amniote implantation, wherein teeth are attached to the jaw bones via either periodontal ligaments (gomphosis) or ossified connective tissue (ankylosis) (Bertin *et al.* 2018), rhynchosaurs exhibit 'ankylothecodont' implantation, which is characterized by the lack of a defined boundary between tooth base and alveolar bone (Chatterjee 1974, Benton 1984, Sethapanichsakul *et al.* 2023b). Early-diverging rhynchosaurs, such as *Howesia*, exhibit multiple tooth rows situated on maxillary and dentary tooth plates. In more deeply nested rhynchosaurs, such as *Rhynchosaurus*, the number of tooth rows is decreased. More deeply nested forms, such as *Hyperodapedon*, are effectively edentulous, instead adopting a shear-like bony blade-and-groove mechanism between the maxilla and dentary. As the most basally diverging rhynchosaur with known cranial material, *Mesosuchus* bears a high potential for

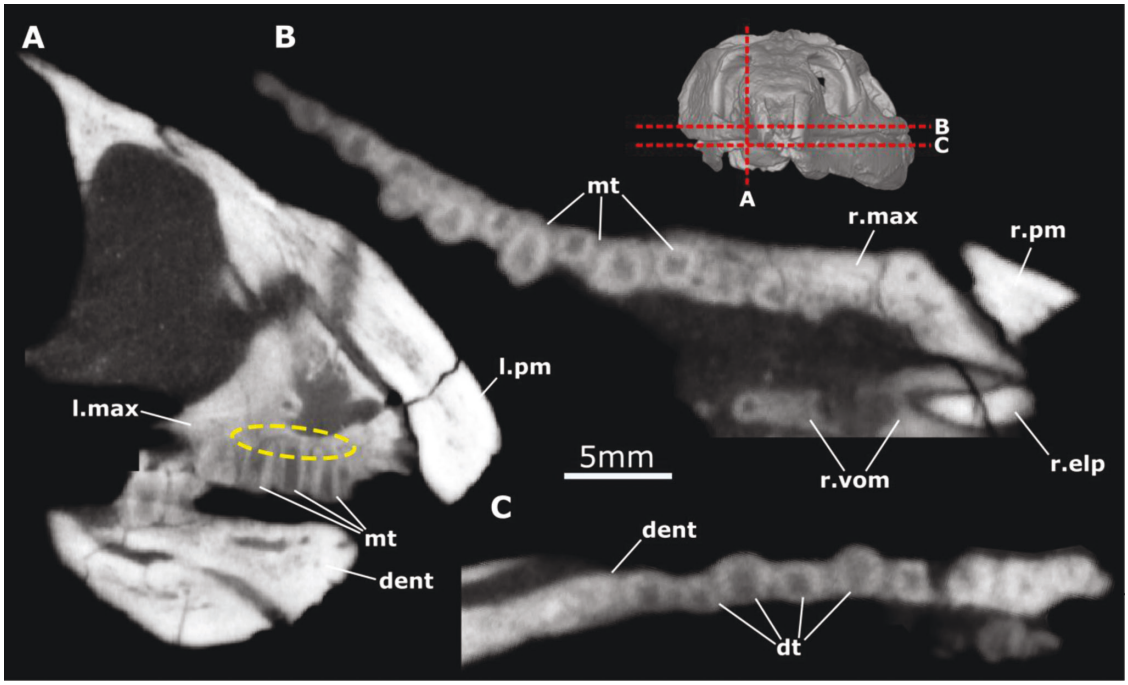

Figure 15. Computed tomography slices of the maxillary and dentary tooth rows of SAM-PK-6536, *Mesosuchus browni*, showing intermedate condition of tooth implantation and arrangement. A, sagittal section of left maxilla; B, transverse section of right maxilla; C, transverse section of right dentary. Dashed yellow line indicates region of seperation between tooth base and alveolar bone of the maxilla.

informing the earliest transformations in rhynchosaur dentition relative to the plesiomorphic amniote states that are conserved among early pan-archosaurs.

Although the maxillary and dentary teeth of *Mesosuchus* are deeply implanted into the bone of the tooth row, there is a narrow area of separation between the basal surface of each tooth and the bone. These observations are congruent with those of Dilkes (1998) and confirm that *Mesosuchus* thus does not possess 'true' ankylothecodonty (Fig. 15A). Dilkes does, however, admit that the typical characteristics of thecodonty also fail to describe the *Mesosuchus* condition adequately. Our interpretation is that *Mesosuchus* exhibits an intermediate morphology between the plesiomorphic thecodont condition of non-rhynchosaurian stem archosaurs and the fully ankylothecodont condition observed in more deeply nested rhynchosaurs.

Our CT data reveal no evidence of a replacement dentition in either the maxilla or the dentary of SAM-PK-6536 (Fig. 15), supporting loss of tooth replacement as a potential synapomorphy of Rhynchosauria.

As suggested by previous authors (Malan 1963, Dilkes 1998), the maxillary tooth row of SAM-PK-6536 exhibits a zig-zag arrangement, perhaps indicative of two tooth rows. Our CT data show that the six anterior teeth are arranged in a single line but begin to split posteriorly into two rows for the remainder of the jaw (Fig. 15B). As in the mode of tooth implantation, what we might be observing here is a transitional state between the plesiomorphic single maxillary tooth row of non-rhynchosaurian stem archosaurs and the multiple tooth rows observed in more derived rhynchosaurs. The dentary in SAM-PK-6536 bears a single line of teeth, reflecting the plesiomorphic condition amongst stem archosaurs (Fig. 15C).

CONCLUSION

Our description of SAM-PK-6536 using computed tomography data adds to the rapidly growing body of early stem archosaur literature. Details of the bones of the rostrum, hard palate, and mandible are now described and figured in detail. Our re-scoring of phylogenetic characters in this taxon provides the most up-to-date and complete matrix for workers interested in reconstructing the relationships of early stem archosaurs. Most importantly, the three-dimensional models and figures produced for this work will be available as a reservoir of phylogenetic characters for use in future analyses and for those interested in building entirely new character matrices. Our interpretation of the anterior palatal anatomy of SAM-PK-6536 raises questions regarding the distribution of the vomeronasal system within the reptile crown and reveals the general lack of understanding regarding the anatomy of the septomaxilla in known stem archosaur specimens. Crucially, an improved understanding of the developmental relationships between the vomeronasal organ and the bones of the anterior palate in extant reptiles will either confirm or disprove our proposed hypothesis that the morphology of the septomaxilla is a correlate for the presence of a vomeronasal organ in fossil taxa.

SUPPLEMENTARY DATA

Supplementary data is available at *Zoological Journal of the Linnean Society* online.

ACKNOWLEDGEMENTS

We would like to thank the members of the Bever Lab, Fernando Torres, E.J. Huang, and Donald Cerio, for their insightful comments that improved the manuscript during preparation. Ralph Molnar kindly provided hard-to-find manuscripts relating to the septomaxilla of *Trilophosaurus*. We thank the University of Texas High-resolution X-ray CT facility for their imaging expertise and help. Thanks are owed to both the reviewer and the handling editor.

AUTHOR CONTRIBUTIONS

W.F., T.R.L., and G.S.B. conceived the project. W.F., P.G., and J.D.W. collected data. W.F. drafted figures. W.F. and G.S.B. drafted the manuscript. R.M.H.S and all other authors contributed to data interpretation, writing, and approved the final manuscript.

CONFLICT OF INTEREST

None declared.

FUNDING

This research was supported by National Science Foundation grant DEB-1947025 to G.S.B and T.R.L.

DATA AVAILIBILITY STATEMENT

The data underlying this article are available at Morphosource at https://www.morphosource.org/concern/media/000616700.

REFERENCES

Albrecht PW. The cranial arteries of turtles and their evolutionary significance. *Journal of Morphology* 1976;**149**:159–82. https://doi.org/10.1002/jmor.1051490203

Allemand R, Abdul-Sater J, Macrì S *et al*. Endocast, brain, and bones: correspondences and spatial relationships in squamates. *Anatomical Record* 2023;**306**:2443–65. https://doi.org/10.1002/ar.25142

Allen BJ, Thomas LS, Benton MJ *et al*. Archosauromorph extinction selectivity during the Triassic–Jurassic mass extinction. *Palaeontology* 2019;**62**:211–24.

Armstrong JA, Gamble HJ, Goldby F. Observations on the olfactory apparatus and the telencephalon of *Anolis*, a microsmatic lizard. *Journal of Anatomy* 1953;**87**:288–307.

Baccari GC, DiMatteo L, Minucci S. The orbital glands of the chelonians *Pseudemys scripta* and *Testudo graeca*: comparative histological, histochemical and ultrastructural investigations. *Journal of Anatomy* 1992;**180**:1–13.

Baeckens S, Herrel A, Broeckhoven C *et al*. Evolutionary morphology of the lizard chemosensory system. *Scientific Reports* 2017;**7**:10141. https://doi.org/10.1038/s41598-017-09415-7

Bellairs AD'A. Observations on the snout of *Varanus*, and a comparison with that of other lizards and snakes. *Journal of Anatomy* 1949;**83**:116–46.

Bellairs AD'A, Boyd JD. The lachrymal apparatus in lizards and snakes.—I. The brille, the orbital glands, lachrymal canaliculi and origin of the lachrymal duct. *Proceedings of the Zoological Society of London* 1947;**117**:81–108.

Bellairs AD'A, Boyd JD. The lachrymal apparatus in lizards and snakes.—II. The anterior part of the lachrymal duct and its relationship with the palate and with the nasal and vomeronasal organs. *Proceedings of the Zoological Society of London* 1950;**120**:269–310.

Benoit J, Ford DP, Miyamae JA *et al*. Can maxillary canal morphology inform varanopid phylogenetic affinities? *Acta Palaeontologica Polonica* 2021;**66**:389–93.

Benton MJT. Tooth form, growth, and function in Triassic rhynchosaurs (Reptilia, Diapsida). *Palaeontology* 1984;**27**:66–8.
Benton MJ. The species Rhynchosaurus, a rhynchosaur (Reptilia, Diapsida) from the Middle Triassic of England. *Philosophical Transactions of the Royal Society of London B: Biological Sciences* 1990a;**328**:213–306.
Benton MJ. End-Triassic. In: Briggs DE, Crowther PR (eds.), *Palaeobiology; a Synthesis*. Oxford: Blackwells, 1990b, 194–8.
Benton MJ. The Triassic reptile *Hyperodapedon* from Elgin: functional morphology and relationships, *Philosophical Transactions of the Royal Society of London B: Biological Sciences* 1983; **302**: 605–718.
Benton MJ, Clark JM. Archosaur phylogeny and the relationships of the Crocodylia. In: Benton MJ (ed). *The Phylogeny and Classification of the Tetrapods, Vol 1: Amphibians and Reptiles*. Oxford: Clarendon Press, 1988, 295–338.
Bertin TJ, Thivichon-Prince B, LeBlanc AR *et al.* Current perspectives on tooth implantation, attachment, and replacement in Amniota. *Frontiers in Physiology* 2018;**9**:1630.
Bertmar G. Evolution of vomeronasal organs in vertebrates. *Evolution* 1981;**35**:359–66. https://doi.org/10.2307/2407844
Bever GS. Postnatal ontogeny of the skull in the extant North American turtle *Sternotherus odoratus* (Cryptodira: Kinosternidae). *Bulletin of the American Museum of Natural History* 2009;**330**:1–97. https://doi.org/10.1206/330.1
Bever GS, Lyson TR, Field DJ *et al.* Evolutionary origin of the turtle skull. *Nature* 2015;**525**:239–42. https://doi.org/10.1038/nature14900
Bhatia MLO. On the arterial system of the lizard *Uromastix hardwickii*. *Journal of Morphology* 1929;**48**:281–316.
Botha J. Biological aspects of the Permian dicynodont *Oudenodon* (Therapsida, Dicynodontia), deduced from bone histology and cross-sectional geometry. *Palaeontologica Africana* 2003;**39**:37–44.
Bouabdellah F, Lessner E, Benoit J. The rostral neurovascular system of *Tyrannosaurus rex*. *Palaeontologia Electronica* 2022;**25**:a3. https://doi.org/10.26879/1178
Broom R. On a new reptile (*Proterosuchus fergusi*) from the Karoo beds of Tarkastad, South Africa. *Annals of the South African Museum* 1903;**4**:159–63.
Broom R. Note on *Mesosuchus browni*, Watson, and on a new South African Triassic pseudosuchian (*Euparkeria capensis*). *Records of the Albany Museum* 1913;**2**:394–6.
Broom R. On the origin of lizards. *Proceedings of the Zoological Society of London* 1925;**95**:1–16. https://doi.org/10.1111/j.1096-3642.1925.tb03338.x
Brusatte SL, Carr TD, Erickson GM *et al.* A long-snouted, multihorned tyrannosaurid from the Late Cretaceous of Mongolia. *Proceedings of the National Academy of Sciences of the United States of America* 2009;**106**:17261–6. https://doi.org/10.1073/pnas.0906911106
Brusatte SL, Nesbitt SJ, Irmis RB *et al.* The origin and early radiation of dinosaurs. *Earth-Science Reviews* 2010;**101**:68–100.
Buchy MC, Frey E, Salisbury SW. The internal cranial anatomy of the Plesiosauria (Reptilia, Sauropterygia): evidence for a functional secondary palate. *Lethaia* 2006;**39**:289–303. https://doi.org/10.1080/00241160600847488
Butler RJ, Ezcurra MD, Montefeltro FC *et al.* A new species of basal rhynchosaur (Diapsida: Archosauromorpha) from the early Middle Triassic of South Africa, and the early evolution of Rhynchosauria. *Zoological Journal of the Linnean Society* 2015;**177**:1030–1030. https://doi.org/10.1111/zoj.12475
Carroll RL. *Noteosuchus* - the oldest known rhynchosaur. *Annals of the South African Museum* 1976;**72**:37–56.
Carroll RL. *Vertebrate Paleontology and Evolution*. NY: W.H. Freeman and Company, 1988.
Cerio DG, Witmer LM. Orbital soft tissues, bones, and allometry: implications for the size and position of crocodylian eyes. *Anatomical Record* 2023;**306**:2537–61. https://doi.org/10.1002/ar.25133
Chatterjee S. A rhynchosaur from the Upper Triassic Maleri Formation of India. *Philosophical Transactions of the Royal Society of London, Series B: Biological Sciences* 1974;**267**:209–61. https://doi.org/10.1098/rstb.1974.0001
Cooper WE. Preliminary reconstructions of nasal chemosensory evolution in Squamata. *Amphibia-Reptilia* 1996;**17**:395–415. https://doi.org/10.1163/156853896x00117
Cotter REMT. Vomeronasal apparatus in *Chrysemys punctata* and *Rana catesbiana*. *Anatomical Record* 1917;**13**:51–67.
Crole MR, Soley JT. Comparative morphology, morphometry and distribution pattern of the trigeminal nerve branches supplying the bill tip in the ostrich (*Struthio camelus*) and emu (*Dromaius novaehollandiae*). *Acta Zoologica* 2016;**97**:49–59. https://doi.org/10.1111/azo.12104
Crosby CE, Humphrey T. Studies of the vertebrate telencephalon. I. The nuclear configuration of the olfactory and accessory olfactory formations and of the nucleus olfactorius anterior of certain reptiles, birds, and mammals. *Journal of Comparative Neurology* 1939;**71**:121–213.
Datta D, Ray S, Bandyopadhyay S. Cranial morphology of a new phytosaur (Diapsida, Archosauria) from the Upper Triassic of India: implications for phytosaur phylogeny and biostratigraphy. *Papers in Palaeontology* 2021;**7**:675–708. https://doi.org/10.1002/spp2.1292
Davidson EH. *The Regulatory Genome: Gene Regulatory Networks in Development and Evolution*. Oxford: Academic Press, 2006.
De Oliveira TM, Oliveira D, Schultz CL *et al.* Tanystropheid archosauromorphs in the Lower Triassic of Gondwana. *Acta Palaeontologica Polonica* 2018;**63**:e0233216.
Dilkes D. The rhynchosaur *Howesia browni* from the Lower Triassic of South Africa. *Palaeontology* 1995;**38**:665–86.
Dilkes D. The Early Triassic rhynchosaur *Mesosuchus browni* and the interrelationships of basal archosauromorph reptiles. *Philosophical Transactions of the Royal Society of London B: Biological Sciences* 1998;**353**:501–41.
Dufeau DL, Witmer LM. Ontogeny of the middle-ear air-sinus system in *Alligator mississippiensis* (Archosauria: Crocodylia). *PLoS One* 2015;**10**:e0137060. https://doi.org/10.1371/journal.pone.0137060
Eisthen HL. Phylogeny of the vomeronasal system and of receptor cell types in the olfactory and vomeronasal epithelia of vertebrates. *Microscopy Research and Technique* 1992;**23**:1–21. https://doi.org/10.1002/jemt.1070230102
Evans SE. The skull of a new eosuchian reptile from the Lower Jurassic of South Wales. *Zoological Journal of the Linnean Society* 1980;**70**:203–64. https://doi.org/10.1111/j.1096-3642.1980.tb00852.x
Evans SE. The skull of lizards and Tuatara. In: Gans C, Gaunt AS, Adler, K (eds.), *Biology of the Reptilia, Vol. 20, The skull of Lepidosauria*. Ithaca: Society for the Study of Amphibians and Reptiles, 2008, 1–347.
Evers SW, Ponstein J, Jansen MA *et al.* A systematic compendium of turtle mandibular anatomy using digital dissections of soft tissue and osteology. *Anatomical Record* 2023;**306**:1228–303.
Ezcurra MD. The phylogenetic relationships of basal archosauromorphs, with an emphasis on the systematics of proterosuchian archosauriforms. *PeerJ* 2016;**4**:e1778. https://doi.org/10.7717/peerj.1778
Ezcurra MD, Butler RJ. Taxonomy of the proterosuchid archosauriforms (Diapsida: Archosauromorpha) from the earliest Triassic of South Africa, and implications for the early archosauriform radiation. *Palaeontology* 2015;**58**:141–70. https://doi.org/10.1111/pala.12130
Ezcurra MD, Fiorelli LE, Trotteyn MJ *et al.* The rhynchosaur record, including a new stenaulorhynchine taxon from the Chañares Formation (upper Ladinian–?lowermost Carnian levels) of La Rioja Province, north-western Argentina. *Journal of Systematic Paleontology* 2020;**18**:1907–38.
Ezcurra MD, Montefeltro F, Butler RJ. The early evolution of rhynchosaurs. *Frontiers in Ecology and Evolution* 2016;**3**:142.
Flynn JJ, Nesbitt SJ, Parrish LR *et al.* A new species of *Azendohsaurus* (Diapsida: Archosauromorpha) from the Triassic Isalo Group of Southwestern Madagascar: cranium and mandible. *Palaeontology* 2010;**53**:669–88.
Gaffney ES. Comparative cranial morphology of recent and fossil turtles. *Bulletin of the American Museum of Natural History* 1979;**164**:69–376.
Gaffney ES. The comparative osteology of the Triassic turtle *Proganochelys*. *Bulletin of the American Museum of Natural History* 1990;**194**:1–263.
Gauthier JA. A cladistic analysis of the higher systematic categories of the Diapsida. D. Phil. Thesis, University of California, 1984.

Gentil AR, Ezcurra MD. Skull osteology of the holotype of the rhynchosaur *Hyperodapedon sanjuansis* (Sill, 1970) from the Upper Triassic Ischigualasto Formation of Argentina. *Anatomical Record* 2022;**305**:1168–200.

Goloboff P, Morales M. TNT version 1.6, with a graphical interface for MacOs and Linux, including new routines in parallel. *Cladistics* 2023;**39**:144–53.

González A, Morona R, López JM. Lungfishes, like tetrapods, possess a vomeronasal system. *Frontiers in Neuroanatomy* 2010;**4**:130.

Gow CE. The morphology and relationships of *Youngina capensis* Broom and Prolacerta *broomi* Parrington. *Palaeontologica Africana* 1974;**8**:89–131.

Gregory JT. *Osteology and Relationships of Trilophosaurus*. University of Texas Publication 1945, **4401**:273–359.

Griffiths EF, Ford DP, Benson RB *et al*. New information on the Jurassic lepidosauromorph *Marmoretta oxoniensis*. *Papers in Palaeontology* 2021;**7**:2255–78. https://doi.org/10.1002/spp2.1400

Grus WE, Zhang J. Origin and evolution of the vertebrate vomeronasal system viewed through system-specific genes. *Bioessays* 2006;**28**:709–18. https://doi.org/10.1002/bies.20432

Halpern M. The organization and function of the vomeronasal system. *Annual Review of Neuroscience* 1987;**10**:325–62. https://doi.org/10.1146/annurev.ne.10.030187.001545

Hancox PJ, Neveling J, Rubidge BS. Biostratigraphy of the *Cynognathus* Assemblage Zone (Beaufort Group, Karoo Supergroup), South Africa. *South African Journal of Geology* 2020;**123**:217–38. https://doi.org/10.25131/sajg.123.0016

Haughton SH. On the reptilian genera *Euparkeria* Broom, and *Mesosuchus* Watson. *Transactions of the Royal Society of South Africa* 1922;**10**:81–8. https://doi.org/10.1080/00359192209519270

Haughton SH. On reptilian remains from the Karoo beds of East Africa. *Quarterly Journal of the Geological Society* 1924;**80**:1–11.

Hillenius WJ, Rehorek SJ. From the eye to the nose: ancient orbital to vomeronasal communication in tetrapods? In: Mason RT, LeMaster MP, Muller-Schwarze D (eds.), *Chemical Signals in Vertebrates, Vol. 10*. Boston: Springer, 2005, 228–41.

Jetz W, Thomas GH, Joy JB *et al*. The global diversity of birds in space and time. *Nature* 2012;**491**:444–8. https://doi.org/10.1038/nature11631

Kaczmarek P, Janiszewska K, Metscher B *et al*. Development of the squamate naso-palatal complex: detailed 3D analysis of the vomeronasal organ and nasal cavity in the brown anole *Anolis sagrei* (Squamata: Iguania). *Frontiers in Zoology* 2020;**17**:28.

Kawabe S, Hattori S. Complex neurovascular system in the dentary of *Tyrannosaurus*. *Historical Biology* 2022;**34**:1137–45. https://doi.org/10.1080/08912963.2021.1965137

King AS, McLelland J. *Outlines of Avian Anatomy*. London: Bailliere Tindall, 1975.

Kishida T, Kubota S, Shirayama Y *et al*. The olfactory receptor gene repertoires in secondary-adapted marine vertebrates: evidence for reduction of the functional proportions in cetaceans. *Biology Letters* 2007;**3**:428–30. https://doi.org/10.1098/rsbl.2007.0191

Klembara J, Hain M, Dobiašová K. Comparative anatomy of the lower jaw and dentition of *Pseudopus apodus* and the interrelationships of species of subfamily Anguinae (Anguimorpha, Anguidae). *Anatomical Record (Hoboken, N. J.: 2007)* 2014;**297**:516–44. https://doi.org/10.1002/ar.22854

Kondoh D, Kitayama C, Kawai YK. The nasal cavity in sea turtles: adaptation to olfaction and seawater flow. *Cell and Tissue Research* 2021;**383**:347–52. https://doi.org/10.1007/s00441-020-03353-z

Korsching S. Aquatic olfaction. In: Munger SD (ed.), *Chemosensory Transduction: the Detection of Odors, Tastes, and Other Chemostimuli*. London: Academic Press, 2016.

Kuhn O. Proganosauria, Bolosauria, Placodontia, Araeoscelidia, Trilophosauria, Weigeltisauria, Millerosauria, Rhynchocephalia, Protorosauria. In: Kuhn O (ed.), *Handbuch der Palaoherpetologie*. Stuttgart: Gustav Fischer, 1969.

Labra A, Niemeyer HM. Intraspecific chemical recognition in the lizard *Liolaemus tenuis*. *Journal of Chemical Ecology* 1999;**25**:1799–811.

Langer MC, Schultz CL. A new species of the Late Triassic rhynchosaur *Hyperodapedon* from the Santa Maria Formation of South Brazil. *Palaeontology* 2000;**43**:633–52. https://doi.org/10.1111/1475-4983.00143

Leitch DB, Catania KC. Structure, innervation, and response properties of integumentary sensory organs in crocodilians. *The Journal of Experimental Biology* 2012;**215**:4217–30. https://doi.org/10.1242/jeb.076836

Lessner EJ, Elsey RM, Holliday CM. A 3D ontogenetic atlas of *Alligator mississippiensis* cranial nerves and their significance for comparative neurology of reptiles. *Anatomical Record* 2022a;**305**:2854–82.

Lessner EJ, Elsey RM, Holliday CM. Ontogeny of the trigeminal system and associated structures in *Alligator mississippiensis*. *Journal of Morphology* 2022b;**283**:1210–30. https://doi.org/10.1002/jmor.21498

Li C, Fraser NC, Rieppel O *et al*. A Triassic stem turtle with an edentulous beak. *Nature* 2018;**560**:476–9. https://doi.org/10.1038/s41586-018-0419-1

Li C, Wu XC, Rieppel O *et al*. Ancestral turtle from the late Triassic of southwestern China. *Nature* 2009;**456**:497–501.

Lingham-Soliar T. Anatomy and functional morphology of the largest marine reptile known, *Mosasaurus hoffmanni* (Mosasauridae, Reptilia) from the Upper Cretaceous, Upper Maastrichtian of the Netherlands. *Philosophical Transactions of the Royal Society of London B: Biological Sciences* 1995;**347**:155–80.

Lohman AH, Smeets WJ. Overview of the main and accessory olfactory bulb projections in reptiles. *Brain, Behavior and Evolution* 1993;**41**:147–55. https://doi.org/10.1159/000113832

López P, Martín J. Sexual selection and chemoreception in lacertid lizards. In: Pérez-Mellado V, Riera N, Perera A (eds.), *The Biology of Lacertid Lizards. Evolutionary and Ecological Perspectives*. Menorca: Institut Menorquí d'Estudis, 2004, 119–37.

Lu Q, Wang K, Lei F *et al*. Penguins reduced olfactory receptor genes common to other waterbirds. *Scientific Reports* 2016;**6**:31671. https://doi.org/10.1038/srep31671

Lyson TR, Bever GS, Bhullar BAS *et al*. Transitional fossils and the origin of turtles. *Biology Letters* 2010;**6**:830–3. https://doi.org/10.1098/rsbl.2010.0371

Lyson TR, Rubidge BS, Scheyer TM *et al*. Fossorial origin of the turtle shell. *Current Biology: CB* 2016;**26**:1887–94. https://doi.org/10.1016/j.cub.2016.05.020

Maddison DR. Phylogenetic methods for inferring the evolutionary history and processes of change in discretely valued characters. *Annual Review of Entomology* 1994;**39**:267–92. https://doi.org/10.1146/annurev.ento.39.1.267

Malan ME. The dentitions of the South African Rhynchocephalia and their bearing on the origin of rhynchosaurs. *South African Journal of Science* 1963;**59**:214–20.

Meek A. On the occurrence of a Jacobson's organ, with notes on development of nasal cavity, lachrymal duct, and harderian gland in *Crocodilus porosus*. *Journal of Anatomy and Physiology* 1893;**27**:151–60.

Miall LC. *The Skull of the Crocodile: a Manual for Students*. London: Macmillan and Co., 1878.

Miedema F, Speikman SNF, Fernandez V *et al*. Cranial morphology of the tanystropheid *Macrocnemus bassanii* unveiled using synchrotron microtomography. *Scientific Reports* 2020;**10**:12412.

Modesto SP, Sues HD. The skull of the Early Triassic archosauromorph reptile *Prolacerta broomi* and its phylogenetic significance. *Zoological Journal of the Linnean Society* 2004;**140**:335–51. https://doi.org/10.1111/j.1096-3642.2003.00102.x

Montefeltro FC, Langer MC, Schultz CL. Cranial anatomy of a new genus of hyperodapedontine rhynchosaur (Diapsida, Archosauromorpha) from the Upper Triassic of southern Brazil. *Earth and Environmental Science Transactions of the Royal Society of Edinburgh* 2010;**101**:27–52. https://doi.org/10.1017/s1755691010009060

Mukherjee D, Ray S. A new *Hyperodapedon* (Archosauromorpha, Rhynchosauria) from the Upper Triassic of India: implications for rhynchosaur phylogeny. *Palaeontology* 2014;**57**:1241–76.

Nakamuta S, Nakamuta N, Taniguchi K *et al*. Histological and ultrastructural characteristics of the primordial vomeronasal organ in

lungfish. *Anatomical Record (Hoboken, N. J.: 2007)* 2012;**295**:481–91. https://doi.org/10.1002/ar.22415
Nesbitt SJ. The early evolution of archosaurs: relationships and the origin of major clades. *Bulletin of the American Museum of Natural History* 2011;**352**:1–292. https://doi.org/10.1206/352.1
Nesbitt SJ, Whatley RL, Irmis RB *et al.* The first discovery of a rhynchosaur from the upper Moenkopi Formation (Middle Triassic) of northern Arizona. *PaleoBios* 2004;**24**:1–10.
Nosotti S. *Tanystropheus longobardicus* (Reptilia, Protorosauria): re-interpretations of the anatomy based on new specimens from the Middle Triassic of Besano (Lombardy, northern Italy). *Memorie della Società Italiana di Scienze Naturali e del Museo Civico di Storia Naturale di Milano* 2007;**35**:1–88.
Oaks JR. A time-calibrated species tree of Crocodylia reveals a recent radiation of the true crocodiles. *Evolution* 2011;**65**:3285–97. https://doi.org/10.1111/j.1558-5646.2011.01373.x
O'Donoghue CH. The blood vascular system of the tuatara, *Sphenodon punctatus*. *Philosophical Transactions of the Royal Society of London B: Biological Sciences* 1921;**210**:175–252.
Oelrich TM. Anatomy of the head of *Ctenosaura pectinata* (Iguanidae). *Miscellaneous Publications Museum of Zoology University of Michigan* 1956;**94**:1–122.
Ollonen J, Da Silva FO, Mahlow K *et al.* Skull development, ossification pattern, and adult shape in the emerging lizard model organism *Pogona vitticeps*: a comparative analysis with other squamates. *Frontiers in Physiology* 2018;**9**:350637.
Osawa G. Beiträge zur Anatomie der Hatteria punctata. *Archiv für Mikroskopische Anatomie und Entwicklungsgeschichte* 1898;**51**:481–691.
Paparella I, Caldwell MW. Cranial anatomy of the Galápagos marine iguana *Amblyrhynchus cristatus* (Squamata: Iguanidae). *Anatomical Record* 2022;**305**:1739–86.
Parks P. 1969. Cranial anatomy and mastication of the Triassic reptile *Trilophosaurus*. M.S. Thesis, University of Texas at Austin, 1969.
Parsons TS. Nasal anatomy and the phylogeny of reptiles. *Evolution* 1959;**13**:175–87. https://doi.org/10.2307/2405871
Polachowski KM, Werneburg I. Late embryos and bony skull development in *Bothropoides jararaca* (Serpentes, Viperidae). *Zoology (Jena, Germany)* 2013;**116**:36–63. https://doi.org/10.1016/j.zool.2012.07.003
Porter WR, Sedlmayr JC, Witmer LM. Vascular patterns in the heads of crocodilians: blood vessels and sites of thermal exchange. *Journal of Anatomy* 2016;**229**:800–24. https://doi.org/10.1111/joa.12539
Porter WR, Witmer LM. Vascular patterns in iguanas and other squamates: blood vessels and sites of thermal exchange. *PLoS One* 2015;**10**:e0139215. https://doi.org/10.1371/journal.pone.0139215
Porter WR, Witmer LM. Avian cephalic vascular anatomy, sites of thermal exchange, and the rete ophthalmicum. *Anatomical Record (Hoboken, N. J.: 2007)* 2016;**299**:1461–86. https://doi.org/10.1002/ar.23375
Porter WR, Witmer LM. Vascular patterns in the heads of dinosaurs: evidence for blood vessels, sites of thermal exchange, and their role in physiological thermoregulatory strategies. *Anatomical Record (Hoboken, N. J.: 2007)* 2020;**303**:1075–103. https://doi.org/10.1002/ar.24234
Rehorek SJ. Squamate Harderian gland: an overview. *The Anatomical Record* 1997;**248**:301–6. https://doi.org/10.1002/(SICI)1097-0185(199707)248:3<301::AID-AR1>3.0.CO;2-S
Rehorek SJ, Elsey RM, Smith TV. Ontogeny of the nasolacrimal apparatus and nasal sensory systems of the American alligator (*Alligator mississippiensis*). *Journal of Morphology* 2022;**283**:1080–93. https://doi.org/10.1002/jmor.21489
Rehorek SJ, Firth BT, Hutchinson MN. The structure of the nasal chemosensory system in squamate reptiles. 1. The olfactory organ, with special reference to olfaction in geckos. *Journal of Biosciences* 2000a;**25**:173–9.
Rehorek SJ, Firth BT, Hutchinson MN. The structure of the nasal chemosensory system in squamate reptiles. 2. Lubricatory capacity of the vomeronasal organ. *Journal of Biosciences* 2000b;**25**:181–90.
Rehorek SJ, Leigh CM, Firth BT. Rate of protein synthesis of the Harderian gland of a skink, *Hemiergis decresiensis*: a preliminary study. *Copeia* 1999;**1999**:526–8. https://doi.org/10.2307/1447505
Rieppel O. Studies on skeleton formation in reptiles: patterns of ossification in the skeleton of *Chelydra serpentina* (Reptilia, Testudines). *Journal of Zoology* 1993a;**231**:487–509. https://doi.org/10.1111/j.1469-7998.1993.tb01933.x
Rieppel OS. Studies on skeleton formation in reptiles. V. Patterns of ossification in the skeleton of *Alligator mississippiensis* DAUDIN (Reptilia, Crocodylia). *Zoological Journal of the Linnean Society* 1993b;**109**:301–25.
Rieppel O, Gauthier J, Maisano J. Comparative morphology of the dermal palate in squamate reptiles, with comments on phylogenetic implications. *Zoological Journal of the Linnean Society* 2008;**152**:131–52. https://doi.org/10.1111/j.1096-3642.2007.00337.x
Rollot Y, Evers SW, Ferreira GS *et al.* Skull osteology, neuroanatomy, and jaw-related myology of the pig-nosed turtle *Carettochelys insculpta* (Cryptodira, Trionychia). *Anatomical Record* 2024;**early view**.
Rollot Y, Lyson TR, Joyce WG. A description of the skull of *Eubaena cephalica* (Hay, 1904) and new insights into the cranial circulation and innervation of baenid turtles. *Journal of Vertebrate Paleontology* 2018;**38**:e1474886. https://doi.org/10.1080/02724634.2018.1474886
Romanoff AL. *The Avian Embryo: Structural and Functional Development*. NY: Macmillan, 1960.
Romer AS. *Osteology of the Reptiles*. Chicago: University of Chicago Press, 1956.
Sales MA, Schultz CL. Paleoneurology of *Teyumbaita sulcognathus* (Diapsida: Archosauromorpha) and the sense of smell in rhynchosaurs. *Palaeontologica Electronica* 2014;**17**:15A.
Scheyer TM, Spiekman NF, Sues HD *et al. Colobops*: a juvenile rhynchocephalian reptile (Lepidosauromorpha), not a diminutive archosauromorph with an unusually strong bite. *Royal Society Open Science* 2020;**7**:192179.
Schoch RR, Sues HD. A Middle Triassic stem-turtle and the evolution of the turtle body plan. *Nature* 2015;**523**:584–7. https://doi.org/10.1038/nature14472
Schulp AS, Mulder EWA, Schwenk K. Did mosasaurs have forked tongues? *Netherlands Journal of Geosciences* 2005;**84**:359–71. https://doi.org/10.1017/s0016774600021144
Schultz CL, Langer MC, Montefeltro FC. A new rhynchosaur from south Brazil (Santa Maria Formation) and rhynchosaur diversity patterns across the Middle–Late Triassic boundary. *PalZ* 2016;**90**:643. https://doi.org/10.1007/s12542-016-0325-5
Schwenk K, Thewissen JGM. Comparative anatomy and physiology of chemical senses in nonavian aquatic reptiles. In: Thewissen JGM, Nummela S (eds.), *Sensory Evolution on the Threshold: Adaptations in Secondarily Aquatic Vertebrates*. Berkeley: University of California Press, 2008; 65–81.
Sennikov AG. New tanystropheids (Reptilia: Archosauromorpha) from the Triassic of Europe. *Paleontological Journal* 2011;**45**:90–104. https://doi.org/10.1134/s0031030111010151
Senter P. Lack of a pheromonal sense in phytosaurs and other archosaurs, and its implications for reproductive communication. *Paleobiology* 2002;**28**:544–50. https://doi.org/10.1666/0094-8373(2002)028<0544:loapsi>2.0.co;2
Sereno PC. Basal archosaurs: phylogenetic relationships and functional implications. *Journal of Vertebrate Paleontology* 1991;**2**:1–53. https://doi.org/10.2307/3889336
Sethapanichsakul T, Coram RA, Benton MJ. New information on the cranial anatomy of the Middle Triassic rhynchosaurian reptile *Bentonyx sidensis*. *Acta Palaeontologica Polonica* 2023a;**68**:53–62.
Sethapanichsakul T, Coram RA, Benton MJ. Unique dentition of rhynchosaurs and their two-phase success as herbivores in the Triassic. *Palaeontology* 2023b;**66**:e12654.
Sheverdyukova HV. Development of the osteocranium in *Natrix natrix* (Serpentes, Colubridae) embryogenesis II: development of the jaws, palatal complex and associated bones. *Acta Zoologica* 2019;**100**:282–91. https://doi.org/10.1111/azo.12253

Sill WD. Functional morphology of the rhynchosaur skull. *Form & Function* 1971;**4**:303–18.
Slabý O. O vyvoji Jacobsonova orginu u ptiku. *Morfologie* 1955;**3**:18–26.
Smith RMH, Botha-Brink J. Burrowing as a survival strategy in the earliest Triassic Karoo Basin, South Africa. *Journal of Vertebrate Paleontology* 2009;**29**:183A.
Sobral G, Müller J. The braincase of *Mesosuchus browni* (Reptilia, Archosauromorpha) with information on the inner ear and description of a pneumatic sinus. *PeerJ* 2019;**7**:e6798. https://doi.org/10.7717/peerj.6798
Sookias RB, Dilkes D, Sobral G *et al*. The craniomandibular anatomy of the early archosauriform *Euparkeria capensis* and the dawn of the archosaur skull. *Royal Society Open Science* 2020;**7**:200116. https://doi.org/10.1098/rsos.200116
Sookias RB, Sullivan C, Liu J *et al*. Systematics of putative euparkeriids (Diapsida: Archosauriformes) from the Triassic of China. *PeerJ* 2014;**2**:e658. https://doi.org/10.7717/peerj.658
Spiekman SNF, Neenan JM, Fraser NC *et al*. The cranial morphology of *Tanystropheus hydroides* (Tanystropheidiae, Archosauromorpha) as revealed by synchrotron microtomography. *PeerJ* 2020;**8**:e10299. https://doi.org/10.7717/peerj.10299
Stocker MR. A new taxon of phytosaur (Archosauria: Pseudosuchia) from the Late Triassic (Norian) Sonsela Member (Chinle Formation) in Arizona, and a critical reevaluation of *Leptosuchus* Case, 1922. *Palaeontology* 2010;**53**:997–1022.
Suárez R, García-González D, De Castro F. Mutual influences between the main olfactory and vomeronasal systems in development and evolution. *Frontiers in Neuroanatomy* 2012;**6**:50.
Sues HD, Fitch AJ, Whatley RL. A new rhynchosaur (Reptilia, Archosauromorpha) from the Upper Triassic of eastern North America. *Journal of Vertebrate Paleontology* 2020;**40**:e1771568. https://doi.org/10.1080/02724634.2020.1771568
Terry RJ. An observation on the development of the mammalian vomer. *The Anatomical Record* 1909;**3**:525–9. https://doi.org/10.1002/ar.1090031002
Voeten DF, Reich T, Araujo R *et al*. Synchrotron microtomography of a *Nothosaurus marchicus* skull informs on nothosaurian physiology and neurosensory adaptations in early Sauropterygia. *PLoS One* 2018;**2018**:e0188509.
von Baczko MB, Desojo JB. Cranial anatomy and palaeoneurology of the archosaur *Riojasuchus tenuisceps* from the Los Colorados Formation, La Rioja, Argentina. *PLoS One* 2016;**11**:e0148575.
von Huene F. *Stenaulorhynchus*, ein Rhynchosauridae der ostrafrikanischen Obertrias. *Nova Acta Leopoldina* 1938;**6**:83–121.
Wagner GP. A research programme for testing the biological homology concept. In: Bock GK, Cardew G (eds.), *Novartis Foundation Symposium 222-Homology*. Chichester: John Wiley and Sons Ltd, 2007; 125–40.
Watson DMS. *Mesosuchus browni*, gen. et spec. nov. *Records of the Albany Museum* 1912;**2**:298–9.
Welman J. The taxonomy of the South African proterosuchids (Reptilia, Archosauromorpha). *Journal of Vertebrate Paleontology* 1998;**18**:340–7. https://doi.org/10.1080/02724634.1998.10011062
Wenzel BM. The olfactory and related systems in birds. *Annals of the New York Academy of Sciences* 1987;**519**:137–49. https://doi.org/10.1111/j.1749-6632.1987.tb36293.x
Werner G. Das Cranium der Brückenechse, *Sphenodon punctatus* Gray, von 58 mm Gesamtlänge. *Zeitschrift für Anatomie und Entwicklungsgeschichte* 1962;**123**:323–68.
Wilson JD, Wisniewski A, Nesbitt S *et al*. Comparative braincase morphology of *Trilophosaurus buettneri* and the early evolution of the pan-archosaurian neurocranium. *Journal of Vertebrate Paleontology* 2022;**42**:e2123712.
Witmer LM. Homology of facial structures in extant archosaurs (birds and crocodilians), with special reference to paranasal pneumaticity and nasal conchae. *Journal of Morphology* 1995;**225**:269–327. https://doi.org/10.1002/jmor.1052250304
Witmer LM. The evolution of the antorbital cavity of archosaurs: a study in soft-tissue reconstruction in the fossil record with an analysis of the function of pneumaticity. *Memoir. Society of Vertebrate Paleontology* 1997;**3**:1–73. https://doi.org/10.2307/3889342
Witmer LM, Ridgely RC. New insights into the brain, braincase, and ear region of tyrannosaurs (Dinosauria, Theropoda), with implications for sensory organization and behavior. *Anatomical Record (Hoboken, N. J.: 2007)* 2009;**292**:1266–96. https://doi.org/10.1002/ar.20983
Wolvaardt FP, Smith RM, Arcucci A. Re-discovery of the Euparkeria bonebed locality (Mid-Triassic) in Aliwal North, South Africa, with an update of the taphonomy and depositional environment. *Palaeontologica Africana* 2023;**56**:89–131.
Wynd BM, Martínez RN, Colombi C *et al*. A review ot vertebrate beak morphologies in the Triassic; a framework to characterize an enigmatic beak from the Ischigualasto Formation, San Juan, Argentina. *Ameghiniana* 2020;**57**:370—387.
Yohe LR, Fabbri M, Hanson M *et al*. Olfactory receptor gene evolution is unusually rapid across Tetrapoda and outpaces chemosensory phenotypic change. *Current Zoology* 2020;**66**:505–14. https://doi.org/10.1093/cz/zoaa051